Check for updates

Global Biogeochemical Cycles

RESEARCH ARTICLE
10.1029/2024GB008102

Trends and Drivers of Terrestrial Sources and Sinks of Carbon Dioxide: An Overview of the TRENDY Project

Stephen Sitch[1], Michael O'Sullivan[1], Eddy Robertson[2], Pierre Friedlingstein[1,3], Clément Albergel[4], Peter Anthoni[5], Almut Arneth[5], Vivek K. Arora[6], Ana Bastos[7], Vladislav Bastrikov[8], Nicolas Bellouin[9], Josep G. Canadell[10], Louise Chini[11], Philippe Ciais[8], Stefanie Falk[12], Ian Harris[13], George Hurtt[11], Akihiko Ito[14], Atul K. Jain[15], Matthew W. Jones[16], Fortunat Joos[17], Etsushi Kato[18], Daniel Kennedy[19], Kees Klein Goldewijk[20], Erik Kluzek[19], Jürgen Knauer[21,22], Peter J. Lawrence[19], Danica Lombardozzi[19], Joe R. Melton[23], Julia E. M. S. Nabel[7], Naiqing Pan[24], Philippe Peylin[8], Julia Pongratz[12,25], Benjamin Poulter[26], Thais M. Rosan[1], Qing Sun[17], Hanqin Tian[24], Anthony P. Walker[27], Ulrich Weber[7], Wenping Yuan[28], Xu Yue[29], and Sönke Zaehle[7]

[1]Faculty of Environment, Science and Economy, University of Exeter, Exeter, UK, [2]Met Office Hadley Centre, Exeter, UK, [3]Laboratoire de Météorologie Dynamique/Institut Pierre-Simon Laplace, CNRS, Ecole Normale, Paris, France, [4]European Space Agency Climate Office, ECSAT, Didcot, UK, [5]Karlsruhe Institute of Technology, Institute of Meteorology and Climate Research/Atmospheric Environmental Research, Garmisch-Partenkirchen, Germany, [6]Canadian Centre for Climate *Modell*ing and Analysis, Environment and Climate Change Canada, Victoria, BC, Canada, [7]Max Planck Institute for Biogeochemistry, Jena, Germany, [8]Laboratoire des Sciences du Climat et de l'Environnement, LSCE/IPSL, CEA-CNRS-UVSQ, Université Paris-Saclay, Gif-sur-Yvette, France, [9]Department of Meteorology, University of Reading, Reading, UK, [10]Global Carbon Project, CSIRO Environment, Canberra, ACT, Australia, [11]Department of Geographical Sciences, University of Maryland, College Park, MD, USA, [12]Ludwig-Maximilians-Universität München, Munich, Germany, [13]National Centre for Atmospheric Science, Climatic Research Unit, School of Environmental Sciences, University of East Anglia, Norwich, UK, [14]Graduate School of Life and Agricultural Sciences, University of Tokyo, Tokyo, Japan, [15]Department of Climate, Meteorology and Atmospheric Sciences (CLiMAS), University of Illinois, Urbana-Champaign, Urbana, IL, USA, [16]Tyndall Centre for Climate Change Research, School of Environmental Sciences, University of East Anglia (UEA), Norwich, UK, [17]Climate and Environmental Physics, Physics Institute and Oeschger Centre for Climate Change Research, University of Bern, Bern, Switzerland, [18]Institute of Applied Energy, Tokyo, Japan, [19]Climate and Global Dynamics Laboratory, National Center for Atmospheric Research, Boulder, CO, USA, [20]Faculty of Geosciences, Copernicus Institute of Sustainable Development, Utrecht University, Utrecht, The Netherlands, [21]Hawkesbury Institute for the Environment, Western Sydney University, Penrith, NSW, Australia, [22]CSIRO Environment, Canberra, ACT, Australia, [23]Climate Research Division, Environment and Climate Change Canada, Victoria, BC, Canada, [24]Department of Earth and Environmental Sciences, Center for Earth System Science and Global Sustainability, Schiller Institute for Integrated Science and Society, Boston College, Chestnut Hill, MA, USA, [25]Max Planck Institute for Meteorology, Hamburg, Germany, [26]Biospheric Sciences Laboratory, NASA GSFC, Greenbelt, MD, USA, [27]Environmental Sciences Division and Climate Change Science Institute, Oak Ridge National Laboratory, Oak Ridge, TN, USA, [28]Institute of Carbon Neutrality, Sino-French Institute for Earth System Science, College of Urban and Environmental Sciences, Peking University, Beijing, China, [29]School of Environmental Science and Engineering, Nanjing University of Information Science and Technology (NUIST), Nanjing, China

Abstract The terrestrial biosphere plays a major role in the global carbon cycle, and there is a recognized need for regularly updated estimates of land-atmosphere exchange at regional and global scales. An international ensemble of Dynamic Global Vegetation Models (DGVMs), known as the "Trends and drivers of the regional scale terrestrial sources and sinks of carbon dioxide" (TRENDY) project, quantifies land biophysical exchange processes and biogeochemistry cycles in support of the annual Global Carbon Budget assessments and the REgional Carbon Cycle Assessment and Processes, phase 2 project. DGVMs use a common protocol and set of driving data sets. A set of factorial simulations allows attribution of spatio-temporal changes in land surface processes to three primary global change drivers: changes in atmospheric CO_2, climate change and variability, and Land Use and Land Cover Changes (LULCC). Here, we describe the TRENDY project, benchmark DGVM performance using remote-sensing and other observational data, and present results for the contemporary period. Simulation results show a large global carbon sink in natural vegetation over 2012–2021, attributed to the CO_2 fertilization effect (3.8 ± 0.8 PgC/yr) and climate (−0.58 ± 0.54 PgC/yr). Forests and semi-arid ecosystems contribute approximately equally to the mean and trend in the natural land sink, and semi-arid ecosystems continue to dominate interannual variability. The natural sink is offset by net

Key Points:

- We quantify and attribute land carbon dynamics to underlying processes at regional scales, contributing bottom-up estimates to RECCAP-2
- Models simulate a contemporary net land sink of 1.7 ± 0.6 PgC/yr, with large opposing effects of CO_2 fertilization and land-use change
- Despite the largest gross fluxes being in the tropics, the largest net land-atmosphere exchange is simulated in the extratropical regions

Supporting Information:

Supporting Information may be found in the online version of this article.

Correspondence to:

S. Sitch,
s.a.sitch@exeter.ac.uk

Citation:

Sitch, S., O'Sullivan, M., Robertson, E., Friedlingstein, P., Albergel, C., Anthoni, P., et al. (2024). Trends and drivers of terrestrial sources and sinks of carbon dioxide: An overview of the TRENDY project. *Global Biogeochemical Cycles*, *38*, e2024GB008102. https://doi.org/10.1029/2024GB008102

Received 10 JAN 2024
Accepted 10 JUN 2024

Author Contributions:

Conceptualization: Stephen Sitch, Pierre Friedlingstein
Formal analysis: Michael O'Sullivan, Eddy Robertson, Ulrich Weber
Methodology: Eddy Robertson, Pierre Friedlingstein, Nicolas Bellouin, Josep G. Canadell, Louise Chini, Philippe Ciais, Ian Harris, George Hurtt, Matthew W. Jones, Kees Klein Goldewijk, Naiqing Pan, Julia Pongratz, Thais M. Rosan, Hanqin Tian, Sönke Zaehle
Resources: Clément Albergel, Peter Anthoni, Almut Arneth, Vivek K. Arora, Vladislav Bastrikov, Nicolas Bellouin, Stefanie Falk, George Hurtt, Akihiko Ito, Atul K. Jain,

© 2024. The Author(s).
This is an open access article under the terms of the Creative Commons Attribution License, which permits use, distribution and reproduction in any medium, provided the original work is properly cited.

Matthew W. Jones, Etsushi Kato, Daniel Kennedy, Kees Klein Goldewijk, Erik Kluzek, Jürgen Knauer, Peter J. Lawrence, Danica Lombardozzi, Joe R. Melton, Julia E. M. S. Nabel, Naiqing Pan, Philippe Peylin, Julia Pongratz, Benjamin Poulter, Thais M. Rosan, Qing Sun, Hanqin Tian, Anthony P. Walker, Ulrich Weber, Wenping Yuan, Xu Yue, Sönke Zaehle
Software: Ulrich Weber
Writing – original draft: Michael O'Sullivan, Eddy Robertson, Pierre Friedlingstein, Louise Chini, Ian Harris, Kees Klein Goldewijk
Writing – review & editing: Clément Albergel, Peter Anthoni, Almut Arneth, Vivek K. Arora, Ana Bastos, Nicolas Bellouin, Josep G. Canadell, Philippe Ciais, Stefanie Falk, George Hurtt, Akihiko Ito, Atul K. Jain, Matthew W. Jones, Etsushi Kato, Daniel Kennedy, Jürgen Knauer, Joe R. Melton, Julia E. M. S. Nabel, Philippe Peylin, Julia Pongratz, Benjamin Poulter, Thais M. Rosan, Qing Sun, Hanqin Tian, Anthony P. Walker, Wenping Yuan, Xu Yue, Sönke Zaehle

emissions from LULCC (-1.6 ± 0.5 PgC/yr), with a net land sink of 1.7 ± 0.6 PgC/yr. Despite the largest gross fluxes being in the tropics, the largest net land-atmosphere exchange is simulated in the extratropical regions.

Plain Language Summary Around one third of human-induced CO_2 emissions are absorbed by land ecosystems and thus act to mitigate climate change. It is essential to understand the processes, ecosystems and regions responsible for this natural carbon sink, to inform on the efficiency of the sinks into the future. These sinks are susceptible to year-to-year variation in response to climate variations and extremes. At the same time deforestation and other forms of land management are changing the land surface, which overall adds significantly to the human-induced CO_2 emissions. There is a need to regularly update our estimate of land carbon dynamics to aid global stock takes for the Paris agreement to avoid dangerous climate change. Here we present an international initiative that on an annual basis assesses "Trends and drivers of the regional scale terrestrial sources and sinks of carbon dioxide" (TRENDY) using computer models of the land carbon cycle. We quantify the land sink during the contemporary period (2012–2021), and attribute to processes, mainly the large opposing effects of CO_2 fertilization enhancing plant productivity and land-use change. Forests and semi-arid ecosystems are largely responsible for the mean and trend in the land sink, with the latter most important for its year-to-year variation.

1. Introduction

The land biosphere plays an important role in the global carbon cycle, as a natural carbon sink for anthropogenic CO_2 and for emissions from land-use and land cover changes (LULCC). The magnitude of the natural land carbon sink (S_{LAND}) has increased along with atmospheric CO_2 and is equivalent to almost one third of total anthropogenic CO_2 emissions, thus providing an important ecosystem service by mitigating climate change (Friedlingstein et al., 2022a). Currently, LULCC emissions (E_{LUC}) contribute to about 11% of total anthropogenic CO_2 emissions (Friedlingstein et al., 2022a) at global scale with important regional variability. Realistic estimates of future land carbon sinks and sources are vital to quantify the remaining carbon budget, that is, the CO_2 that society can still emit to stay within the targets of 1.5°C or well below 2°C considered by the UN Paris Agreement. This information is critical to understand the efficiency of land ecosystems to sequester carbon in the future (Arora et al., 2020). While the global magnitude of the net land-atmosphere carbon exchange is well known and observable (Ruehr et al., 2023), key challenges remain in identifying its geographical location, ecosystems and processes (e.g., split between S_{LAND} and E_{LUC}) responsible for variability and trends, and the timescales at which they act (Pongratz et al., 2021). Hence the need for process-based models to inform on attribution.

Different families of land models are used in carbon cycle assessments, including here in the TRENDY project. Contemporary Dynamic Global Vegetation Models (DGVMs) have developed over the past 30 years, and have their roots in the disciplines of biogeography, biogeochemistry, forest gap dynamics, and land surface modeling (LSMs) (Fisher et al., 2014; Prentice et al., 2007). We use the broad term DGVM as it encapsulates dynamic modeling of vegetation and associated biogeochemical cycling at global scales. Several of the TRENDY DGVMs are also LSMs. LSMs are important tools to study the physical and biogeochemical land surface processes at sub-daily timescales and can be coupled into Earth System Models. During the 1990s, LSMs were compared against each other for the first time in the Project for Intercomparison of Land Surface Schemes (PILPS) (Henderson-Sellers et al., 1993) in terms of their ability to simulate physical processes. The Coupled Model Intercomparison Project (CMIP) also started at around this time, focusing on coupled ocean-atmosphere general circulation models, and later the Coupled Climate-Carbon Cycle MIP (C4MIP) (Friedlingstein et al., 2006). The first biogeochemistry-focused MIPs were designed to synthesize results on land carbon dynamics, provide consensus, identify uncertainties, and quantify the role of individual processes to the land carbon cycle. These included the Net Primary Production MIP (Cramer et al., 2001) and two concurrent projects: the Vegetation-Ecosystem Modeling and Analysis Project (VEMAP) (Melillo et al., 1995), and the Carbon Cycle Model Linkage Project (CCMLP) (Heimann et al., 1998; McGuire et al., 2001). These early MIPs laid the foundation for subsequent DGVM intercomparisons, based on the idea of provision of a common simulation protocol, timelines, and driving data sets. McGuire et al. (2001) pioneered the factorial simulation approach whereby models were driven with a different combination of time-varying and fixed environmental forcing drivers. This approach aims to attribute change in any model simulated quantity to the underlying forcing drivers and their interactions. In addition,

19449224, 2024, 7, Downloaded from https://agupubs.onlinelibrary.wiley.com/doi/10.1029/2024GB008102 by University Of Illinois At, Wiley Online Library on [22/07/2024]. See the Terms and Conditions (https://onlinelibrary.wiley.com/terms-and-conditions) on Wiley Online Library for rules of use; OA articles are governed by the applicable Creative Commons License

19449224, 2024, 7, Downloaded from https://agupubs.onlinelibrary.wiley.com/doi/10.1029/2024GB008102 by University Of Illinois At, Wiley Online Library on [22/07/2024]. See the Terms and Conditions (https://onlinelibrary.wiley.com/terms-and-conditions) on Wiley Online Library for rules of use; OA articles are governed by the applicable Creative Commons License

identification of sources of model uncertainty allows to quantify knowledge and data gaps, and thus guide future model improvements as well as inform empirical, monitoring and observational needs.

The TRENDY Project (Sitch et al., 2015), uses the same factorial approach. TRENDY is an international MIP which contributes regional and global Net Biome Production (NBP) estimates to the annual Global Carbon Budget (GCB) assessments (e.g., Friedlingstein et al., 2022a), with data available to the wider scientific community for numerous additional analyses on land biogeochemistry. TRENDY models contributed to the first GCB assessment (Le Quéré et al., 2009) and the Regional Carbon Cycle Assessment and Processes project, phase 1 (RECCAP-1) (Sitch et al., 2015). These early studies focused on diagnosing the natural land carbon sink, and in more recent years the protocol has expanded to include LULCC to estimate associated E_{LUC}. As a community TRENDY-v1 started in 2009, and has been repeated every year since 2013 (TRENDY-v2), through to TRENDY-v11 in 2022 using updated and extended forcing data sets. Throughout this period the protocol has been developed and refined.

The aim of this paper is to document the recent protocol as used for TRENDY v11, including an updated description of the standard set of factorial simulations, underlying environmental forcing data sets up to the year 2021, and to present results for the contemporary period beyond those presented in GCB2022 (Friedlingstein et al., 2022a), and over 10 geographical regions used in RECCAP2.

2. Methods

2.1. Data Sets

A description of the forcing data sets is given below and summarized in Table S1 of Supporting Information S1. This includes a general description valid for TRENDY versions since Sitch et al. (2015) and where necessary specific additional information for TRENDY-v11/GCB2022.

Our general modeling approach is to use the most up-to-date historical data sets available and pre-processed by May/June each year to be able to run the DGVMs in July/August. Our choice of climate forcing is based on our need to run DGVMs with high-temporal fidelity (diel cycle) observation-based climate over long, century timescales with low latency. We need gridded forcing data covering the period 1900 until the end of the previous year, that is, for TRENDY-v11 until the end of 2021. In each new annual cycle of TRENDY these data are updated by the addition of 1 year, and retrospectively, as new historical meteorological station data become available and/or blending and interpolation methodologies change. Given the multi-decade to century timescales of carbon legacy fluxes associated with land use change (e.g., soil carbon stock change with deforestation), our LULCC forcing also needs to be global, spatially explicit (transformed onto a common grid with the climate forcing) and cover multiple centuries, that is, prior to the satellite era, for example, from 1700 onwards. Some underlying data sets are either not available every year, for example, data from the global Forest Resources Assessments (FRA), and/or are not updated in time for the GCB annual assessments, for example, the Food and Agricultural Organization of the United Nations (FAO) land-use statistics. Thus, we need to make extrapolations in time, and in some GCB years, for simplicity, FAO data were not updated at all.

2.1.1. Global Atmospheric CO_2

A 1700–2021 monthly time-series, derived by combining ice core CO_2 data with monthly observations of CO_2 concentration from NOAA stations since 1958, is prepared for the annual GCB assessments. Data from March 1958 onwards are based on monthly averages from Mauna Loa (MLO) and South Pole (SPO) atmospheric monitoring stations, provided by NOAA's Earth System Research Laboratory http://www.esrl.noaa.gov/gmd/ccgg/trends/. When no SPO data are available (including for the entire period 1959–1975 and some months after 1975), the SPO time series is gap-filled based on the trend in divergence of SPO from MLO across years and the climatological mean monthly difference between SPO from MLO during the period 1976–2014. Data prior to March 1958 are estimated with a cubic spline fit to CO_2 concentrations from air trapped in ice cores (Joos & Spahni, 2008). Annual mean fields are generated from these monthly data to force the DGVMs.

2.1.2. Climate Forcing

The Climatic Research Unit (CRU) monthly historical climate data at 0.5° spatial resolution are based on a synthesis of meteorological station data ("CRU TS") and are available for the period 1901–2021, or to the

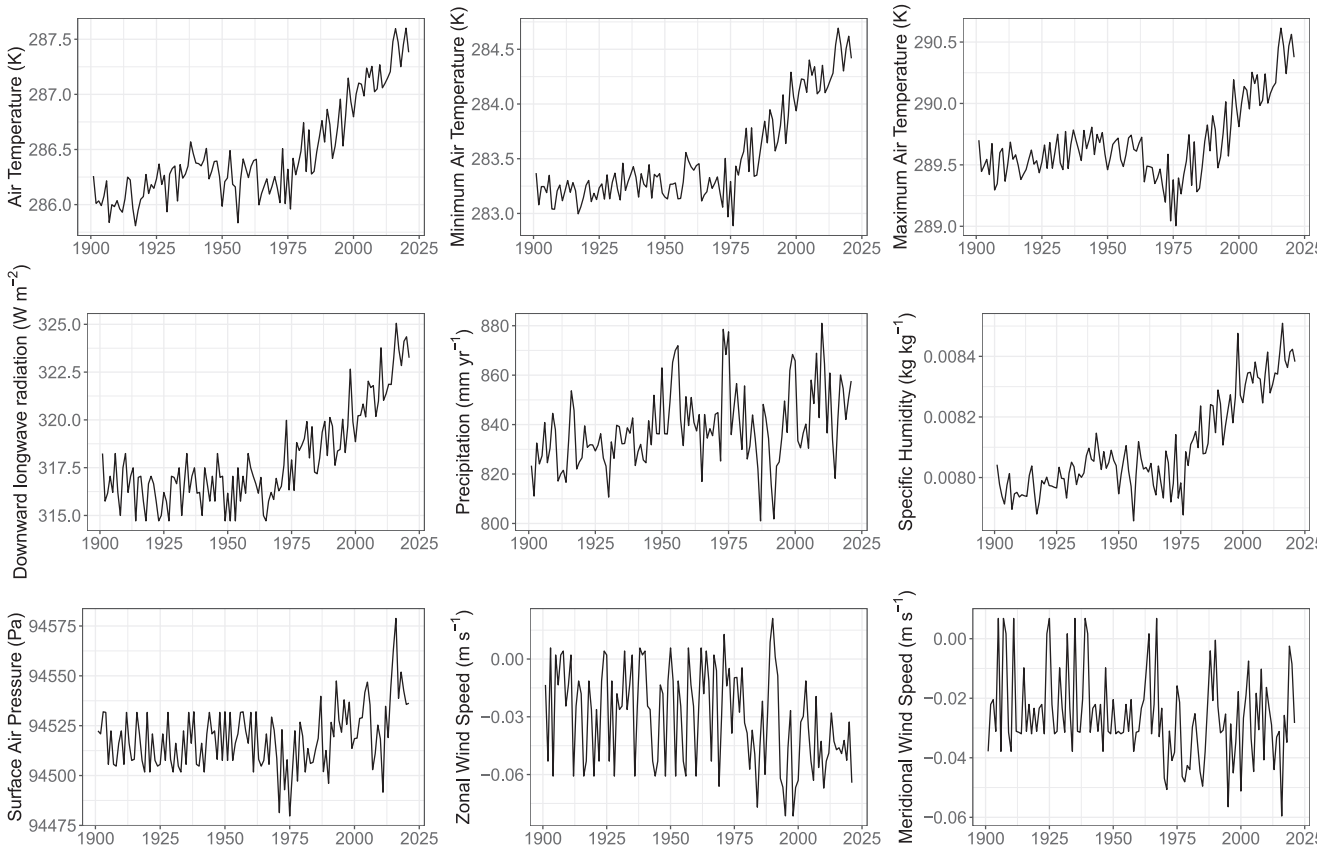


Figure 1. Temporal variation of all meteorological driving variables (global means over land presented).

previous year of the simulations for more recent releases. These data are selectively merged with sub-daily climate data from a new generation reanalysis product, JRA-55 (Japanese 55-year Reanalysis), which are available for the period 1958–2021. The blended product yields a composite 0.5 degree CRUJRA 6-hourly historical climate forcing data set from 1901 to 2021 for the following climate variables: minimum, maximum, and mean air temperature (t_{min}, t_{max}, tmp); precipitation (pre), specific humidity (spfh), pressure (pres), wind speed (u and v-components, ugrd, vgrd) and downward longwave radiation (dlwrf) (Figure 1). The model resolution of JRA is T319 Gaussian grid (approximately 0.56°), which is close to 0.5° spatial resolution of the CRU data set.

The procedure for blending JRA with CRU data is described as follows. All JRA-55 data are regridded to the CRU 0.5° grid using NCL routines (based on ESMF routines) and masked to give a land-only (excluding Antarctica) data set. The time series for each variable is obtained by scaling the 6-hourly data simulated in the Japanese Reanalysis (JRA; Kobayashi et al., 2015) so that their monthly means or totals match those in the CRU TS v4.03 (and later versions) data set (Harris et al., 2020). This procedure, termed "alignment" hereafter, is applied to T_{mean}, T_{max}, T_{min}, Spfh and Pre: T_{min} and T_{max} are aligned with CRU TS Mean Temperature (TMP) and Diurnal Temperature Range; T_{mean} is aligned with TMP; Spfh is aligned with CRU TS Vapor Pressure (VAP, converted to Specific Humidity); Pre is aligned with CRU TS Precipitation (PRE). The other five variables (pres, ugrd, vgrd, dlwrf, dswrf) in the JRA-55 data are not aligned with CRU TS. For the time period 1958–2021 for which JRA-55 data are available they are blended with the CRU TS data using the procedure described above. For the time period 1901–1957, for which the CRU TS data are available but the JRA-55 data are not, randomly chosen (but now fixed - to allow repeatability) years from JRA-55 are chosen from the period 1958–1967 and assigned to the years 1901–1957, thus providing high-frequency variability in the earlier period. Each month in that period is then aligned with the appropriate CRU TS monthly value from 1901 to 1957, as above.

19449224, 2024, 7, Downloaded from https://agupubs.onlinelibrary.wiley.com/doi/10.1029/2024GB008102 by University Of Illinois At, Wiley Online Library on [22/07/2024]. See the Terms and Conditions (https://onlinelibrary.wiley.com/terms-and-conditions) on Wiley Online Library for rules of use; OA articles are governed by the applicable Creative Commons License

19449224, 2024, 7, Downloaded from https://agupubs.onlinelibrary.wiley.com/doi/10.1029/2024GB008102 by University Of Illinois At, Wiley Online Library on [22/07/2024]. See the Terms and Conditions (https://onlinelibrary.wiley.com/terms-and-conditions) on Wiley Online Library for rules of use; OA articles are governed by the applicable Creative Commons License

2.1.3. Revised Radiation Fields

Vegetation productivity is sensitive to both the quantity and quality of light. The latter relates to the scattering of incoming shortwave radiation through the atmosphere during cloudy skies and/or through aerosols in the atmosphere. Scattered light, that is, diffuse light conditions, provides a more uniform distribution of light through the vegetation canopy and can thus enhance photosynthesis in shaded leaves in the sub-canopy layers which are typically light-limited (Roderick et al., 2001). The impact of diffuse radiation on the simulated global land carbon sink was first evaluated in the framework of the JULES land model (Mercado et al., 2009). Mercado et al. (2009) found that the use of diffuse radiation for photosynthesis enhances the global land carbon sink by approximately one-quarter between 1960 and 1999. As more DGVMs include the ability to use both direct and diffuse radiation within their photosynthesis modules, a time series of diffuse radiation has been provided as part of the TRENDY protocol since TRENDY-v10/GCB2021 (Friedlingstein et al., 2022b). In TRENDY-v11, CABLE-POP, CLM5.0, JULES-ES, and YIBs used the diffuse fraction information. A separate study using two DGVMs and this diffuse radiation time series was also published (O'Sullivan et al., 2021). Here we summarize the diffuse forcing data set with more detailed information in O'Sullivan et al. (2021).

Six hourly fields of the diffuse fraction of surface shortwave fluxes were generated over the period 1901–2021 (Figure S1 in Supporting Information S1). A detailed evaluation of the data set against in situ radiation data is performed in O'Sullivan et al. (2021). Radiative transfer calculations are based on monthly averaged distributions of tropospheric and stratospheric aerosol optical depth, and 6-hourly distributions of cloud fraction. The procedure followed is described in the Methods section of Mercado et al. (2009), but with updated input data sets. Surface radiative fluxes account for aerosol-radiation interactions from both tropospheric and stratospheric aerosols, and aerosol-cloud interactions from tropospheric aerosols, except mineral dust. Tropospheric aerosols are also assumed to exert interactions with clouds. The radiative effects of those aerosol-cloud interactions are assumed to scale with the radiative effects of aerosol-radiation interactions of tropospheric aerosols, using regional scaling factors derived from HadGEM2-ES.

The time series of speciated tropospheric aerosol optical depth is taken from the historical and RCP8.5 simulations by the HadGEM2-ES climate model (Bellouin et al., 2011). To correct for biases in HadGEM2-ES, tropospheric aerosol optical depths are scaled over the whole period to match the global and monthly averages obtained over the period 2003–2020 by the CAMS Reanalysis of atmospheric composition (Inness et al., 2019), which assimilates satellite retrievals of aerosol optical depth.

The time series of stratospheric aerosol optical depth is taken from the climatology by Sato et al. (1993), which has been updated to 2012. The stratospheric aerosol optical depth for years 2013–2021 was assumed to be the same as for a normal year (2010), which saw background stratospheric aerosol concentration, with no large volcanic eruption or lingering effects of prior volcanic eruptions. This assumption is supported until at least 2016 included by the Global Space-based Stratospheric Aerosol Climatology time series (1979–2016; Thomason et al., 2018).

Solar radiation is assumed to be 100% diffuse in cloudy skies. Atmospheric constituents other than aerosols and clouds are set to a constant standard mid-latitude summer atmosphere, as their variations do not affect the diffuse fraction of surface shortwave fluxes. Each grid is partitioned into cloudy and cloud free fractions at 6-hourly intervals using JRA-55 data, scaled to match CRU monthly observations.

2.1.4. Land Use Change

The earliest approaches to simulate the effect of land use change in DGVMs (McGuire et al., 2001) used gridded annual data sets of cropland coverage and a rule-based approach, adopted from book-keeping models (Houghton et al., 1983), to simulate the fate of deforested carbon over land where natural vegetation is converted to cropland. Newer data sets now include, in addition to changes in cropland area, changes in pasture and grazing area and detailed sub-grid transitional information between vegetation cover classes which allows to represent practices such as shifting cultivation. Models have also improved their representation of land-use change processes, including incorporating wood harvest, shifting cultivation, grazing, crop harvesting, and cropland management, although the individual capabilities vary between models (Arneth et al., 2017; Pongratz et al., 2017). The use of agricultural area change (including cropland and pasture) data sets is an indirect way to infer change in area of natural ecosystems, for example, forest loss and gain due to deforestation and secondary forest regrowth. The

advantage of using information on changes in agricultural area and wood harvest as compared to using directly information on area and state of forest and other natural vegetation types is that anthropogenic and natural drivers are cleanly separated. Time-varying, spatially explicit data sets that are used to represent land use change in models are based on annual land use and population data from History Database of the Global Environment v3.3 (HYDE 3.3), land use states and transitions produced by updates to the Land Use Harmonization v2 model (LUH2-GCB; Chini et al., 2021), and Food and Agriculture Organization (FAO) wood harvest data. LUH2 has been developed for the purpose of driving land models as part of the CMIP endeavor and has been extended in scope to match progress in LULCC description in the DGVMs.

2.1.4.1. HYDE3.3

HYDE combines historical population estimates and model algorithms to generate spatially explicit, temporally varying maps of land use categories (Klein Goldewijk, Beusen, et al., 2017), for the period 10,000 Before the Common Era (BCE) to 2017 Common Era (CE) period. The land use maps are based on an allocation algorithm that uses country totals from the Food and Agricultural Organization of the United Nations statistical data (FAOSTAT) of "Arable land and permanent crops" and "Permanent meadows and pastures" (or "grazing land" in HYDE) for the 1961 to present period (FAO, 2020a), and other historical census data supplemented with per-capita land use estimates for the pre-1960 period. HYDE uses the European Space Agency Climate Change Initiative (ESA-CCI) (Plummer et al., 2017) medium-resolution land cover data set (ESA, 2016; Harper et al., 2023), to spatially allocate the FAO land use areas for the present-time (1992–2018), which are gradually replaced by a combination of normalized proxies (climate, soil fertility, distance to water, slope, population density) to allocate land use area for the past.

To further inform land cover change in DGVMs, the grazing land use category is subdivided based on the intensity of use; grazing in rangelands (extensive grazing on the drier natural ecosystems), managed pastures (intensive grazing or mowing, on any natural vegetation type) and converted rangeland (forests converted to rangelands in areas with low human population density). ESA CCI land cover data are used to constrain the spatial allocation of cropland and grazing land on an annual basis for the period 1992–2017 (Klein Goldewijk, Dekker, et al., 2017). FAO agricultural statistics are used until 2017, and for TRENDY-v11 we extrapolated these data using the trend from 2012 to 2017 forward in time (see LUH2-GCB section).

However, using FAO statistics and its extrapolation may not be appropriate for capturing trends and variability in countries that have changed reporting methodologies without retrospective data revision or experienced recent rapid land-use change. For example, China (Yu et al., 2022) and Brazil (Rosan et al., 2021), have witnessed a recent increase in reforestation/afforestation and deforestation, respectively. This is a major source of uncertainty in GCB assessments (Bastos et al., 2020; Rosan et al., 2021). For Brazil, in TRENDY-v11 we have replaced the FAO state-level data for Brazil's cropland and grazing land with those derived from the in-country land cover data set MapBiomas (collection 6) for the 1985–2020 period (Souza et al., 2020). Note, ESA-CCI spatially explicit land cover maps are still used to spatially allocate the total country area following HYDE methodology. For Brazil, an estimate of land use change for the year 2021 is based on the trend 2015–2020 from the total areas calculated from MapBiomas. The pre-1985 period is scaled with the per capita numbers from 1985, so ensuring a smooth transition. The land use areas in the HYDE framework are computed at a 5-arc min spatial resolution and aggregated to a 0.25-degree resolution for use in LUH2.

2.1.4.2. LUH2-GCB

Gridded HYDE data on agricultural area (cropland and grazing area), population data until 2017 (2020 for Democratic Republic of the Congo, and 2022 for Brazil) and national wood harvest production data from FAO (2020b) are then used as input to the process that generates the updated Land-Use Harmonization 2 (LUH2-GCB) data set (Chini et al., 2021; Hurtt et al., 2019a, 2019b, 2020). LUH2 harmonizes multiple datastreams into a single 0.25-degree spatial resolution data set of land-use transitions for 12 land-use states, the age and area of recovering secondary lands, wood harvest area, and agricultural management practices such as irrigated area and synthetic nitrogen fertilizer application (Hurtt et al., 2020). The 12 LUH2 land-use states are cropland (C3 annuals, C4 annuals, C3 perennials, C4 perennials, and C3 N-fixers), grazing land (managed pasture and rangeland), urban land, primary land (both forested and non-forested), and secondary land (forested and non-forested).

19449224, 2024, 7, Downloaded from https://agupubs.onlinelibrary.wiley.com/doi/10.1029/2024GB008102 by University Of Illinois At, Wiley Online Library on [22/07/2024]. See the Terms and Conditions (https://onlinelibrary.wiley.com/terms-and-conditions) on Wiley Online Library for rules of use; OA articles are governed by the applicable Creative Commons License

19449224, 2024, 7, Downloaded from https://agupubs.onlinelibrary.wiley.com/doi/10.1029/2024GB008102 by University Of Illinois At, Wiley Online Library on [22/07/2024]. See the Terms and Conditions (https://onlinelibrary.wiley.com/terms-and-conditions) on Wiley Online Library for rules of use; OA articles are governed by the applicable Creative Commons License

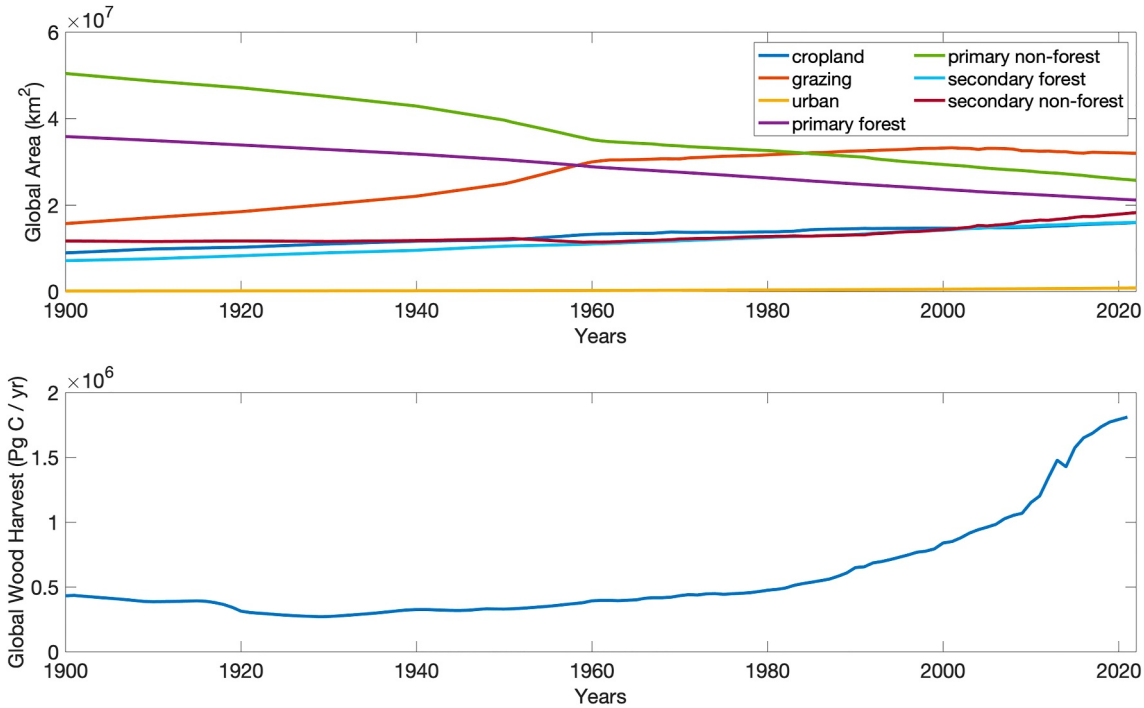


Figure 2. (a) Historical land use and land cover change from LUH2 based on HYDE3.3 from 1900 to 2021. (b) Temporal variation in global wood harvest over the same time period.

In TRENDY-v11, for all countries except Brazil and the Democratic Republic of the Congo, after the year 2017, LUH2-GCB linearly extrapolates on a per gridcell basis the cropland, pasture, and urban data, based on the trend over the previous 5 years (2012–2017), to generate data for years 2018–2022. For gridcells within the Democratic Republic of the Congo this is needed only from 2020 until the year 2022. For gridcells within Brazil, LUH2-GCB uses the annual HYDE data as it is provided for the full length of the simulation. Land-use states are available for the period 850–2022 (Figure 2a), and land-use transitions for the period 850–2021 (Chini et al., 2021). Extrapolation using the trend over the previous 5 years is a pragmatic approach to enable necessary extension of the LULCC data sets. After successful adoption of mapbiomas for Brazil, we envisage the adoption of low latency, time-varying Earth Observation based maps of LULCC moving forward.

For the wood harvest inputs to LUH2-GCB, we use annual FAO wood harvest data from 1961 to 2019, and linearly extrapolate to the year 2022 because FAO updates were not available (Figure 2b). Wood harvest patterns are constrained with Landsat-based tree cover loss data (Hansen et al., 2013). HYDE population data are used to extend this time series back in time prior to 1961, along with data from Zon and Sparhawk (1923) which is used to specify national wood harvest demands in the year 1920. Some DGVMs use in addition to land-use transition data, directly information on wood harvest.

LUH2-GCB data were provided in three separate files (for the states, transitions, and management data layers). A full set of LUH2-GCB diagnostics are given in Table S1 of Supporting Information S1. Figure 3 shows improved diagnostics in the LUH2-GCB2022 data set when compared with reference data for two important regions/variables: cropland in the Democratic Republic of the Congo, and for recent primary forest loss over the satellite era in Amazonian Brazil.

2.1.4.2.1. Application of LUH2 in DGVMs: Conversion to Pasture/Rangeland

The LUH2 methodology uses the cropland, managed pasture, rangeland, and urban layers from HYDE. Natural vegetation is cleared for croplands. DGVM groups in the past have requested more information on whether natural vegetation is lost in conversion to managed pasture or rangeland, since only the former is typically associated with a change in land cover from natural vegetation to managed grassland. The LUH2 simple guidelines provided at https://luh.umd.edu/data.shtml (Ma et al., 2020) state: "*all natural vegetation should be*

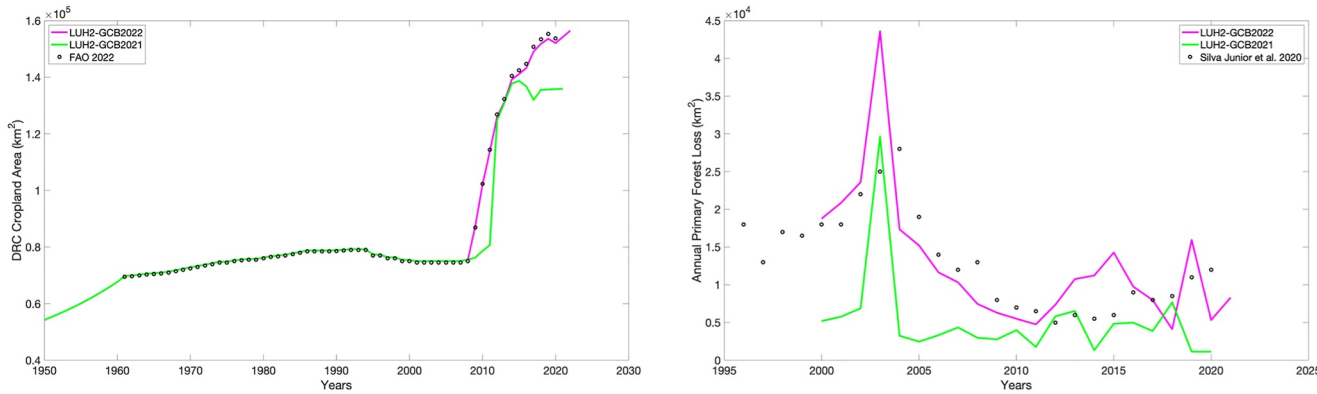


Figure 3. (a) Cropland area for the Democratic Republic of Congo for FAO 2022, LUH2-GCB2022, and LUH2-GCB2021 and (b) annual primary forest loss for Amazonian Brazil from satellite-based PRODES (INPE, 2020; Silva Junior et al., 2020), LUH2-GCB2022, and LUH2-GCB2021.

cleared for managed pasture, and only cleared for rangeland if it is forested." Using this rule/guideline, together with the forest layer from LUH2, gives maps of forest area, carbon density, and carbon emissions. Models can have static or dynamic natural vegetation but all use prescribed geographical distribution of cropland and grazing land (defined as the sum of managed pasture and rangeland). These LULCC data sets are common to all the DGVMs, but their implementation differs depending on the land-use processes and functionalities in individual models (Arneth et al., 2017; Table 1). LUH2-GCB provides fractional gridcell information on land-use states and their transitions that enables DGVM simulation of sub-grid transitions and gross LUC carbon fluxes, for example, associated with deforestation and forest regrowth from shifting cultivation within the same gridcell, and permanent deforestation and forest (re-)growth due to afforestation/reforestation. However, some DGVMs are only able to simulate net E_{LUC}, and thus rely on the subset of net agricultural area changes based on HYDE, whereas others can simulate gross E_{LUC}, that is, including sub-grid cell transitions/shifting cultivation, which require in addition the land-use transition information from LUH2 (Table 1).

2.1.5. Nitrogen Deposition and Fertilizer

A major effort has been made to also represent nutrient cycles in DGVMs, first with the inclusion of a Nitrogen (N) cycle (Thornton et al., 2007; Zaehle & Friend, 2010) and more recently a phosphorous cycle (Goll et al., 2017; Y. P. Wang et al., 2007, 2010, X. Yang et al., 2014). Broadly, high latitude ecosystems with lower nitrogen mineralization rates in cold environments may be nitrogen limited, whereas highly weathered tropical soils are thought to be primarily P limited. In a modeling study Zaehle et al. (2010), simulated a reduction in the global CO_2 fertilization effect in land ecosystems counteracted by a reduced positive climate-carbon cycle feedback with inclusion of a nitrogen cycle. N deposition fields can also alleviate potential N limitation. Carbon-nitrogen cycle DGVMs (Table 1) therefore need historical gridded forcing data on nitrogen deposition and fertilizer application.

Nitrogen fertilizer input data sets are available via the NMIP and NMIP2 projects (Tian et al., 2018, 2019, 2022). Manure is an organic fertilizer (animal waste put on fields), and is important from the N-cycle perspective, because it is one of the natural fertilizer sources. However, since manure is organic N, it must be taken from other organic N sources in a model which causes problems with mass balance without representation of other relevant processes. Doing this incorrectly will influence the simulated C and N cycle. For TRENDY, DGVMs are thus recommended not to include manure application over croplands. Artificial inorganic N fertilizer application started after 1910 (the Haber-Bosch process was developed in the early 20th century), and thus DGVMs assume zero N fertilizer for years 1700–1910. Recently gridded N inorganic fertilizer application rates have been updated to 2020 (Tian et al., 2022). For TRENDY-v11 DGVMs assume N fertilizer application rates remain unchanged in years 2020–2021 (Tian et al., 2022).

For nitrogen deposition (Ndep), DGVMs use historical N-deposition rates for the period 1850–2014 and then transition to the future RCP8.5 N-deposition scenario for the period 2015–2021 (Hegglin et al., 2016). N deposition is available only from 1850, and DGVMs assume N deposition at the 1850 value for years 1700–1850.

19449224, 2024, 7, Downloaded from https://agupubs.onlinelibrary.wiley.com/doi/10.1029/2024GB008102 by University Of Illinois At, Wiley Online Library on [22/07/2024]. See the Terms and Conditions (https://onlinelibrary.wiley.com/terms-and-conditions) on Wiley Online Library for rules of use; OA articles are governed by the applicable Creative Commons License

19449224, 2024, 7, Downloaded from https://agupubs.onlinelibrary.wiley.com/doi/10.1029/2024GB008102 by University Of Illinois At, Wiley Online Library on [22/07/2024]. See the Terms and Conditions (https://onlinelibrary.wiley.com/terms-and-conditions) on Wiley Online Library for rules of use; OA articles are governed by the applicable Creative Commons License

Table 1
Adapted From Table A1 Friedlingstein et al. (2022a)

Model	CABLE-POP	CLASSIC	CLM5.0	DLEM	IBIS	ISAM	JSBACH	JULES
Processes relevant to SLAND								
Fire	N	Y	Y	N	Y	N	Y	Y
N cycle	Y	N[a]	Y	Y	N	Y	Y	Y
P cycle	N	N		N	N	N	N	N
Ecosystem Demography	Y	N		N	N	N	N	N
Dynamic natural PFT coverage	N	N[a]			Y			Y
Processes relevant to ELUC								
Wood Harvest	Y	N	Y	Y	Y	Y	Y	N
Shifting Cultivation/Subgrid transitions	Y	N	Y	N	N	N	Y	N
Crop harvest	Y	Y	Y	Y	Y	Y	Y	Y
Peat fires	N	N	Y	N	N	N	N	N
Tillage	N	Y	N	N	N	N	N	N
Irrigation	N	N	Y	Y	N	Y	N	N
Erosion	N	N	N	Y	N	N	N	N

Model	LPJ	LPJ-GUESS	LPX	OCN	ORCHIDEE	SDGVM	VISIT	VISIT-NIES	YIBS
Processes relevant to SLAND									
Fire	Y	Y	Y	N	N	Y	Y	Y	N
N cycle	N	Y	Y	Y	Y	Y[b]	N	N	N
P cycle	N	N	N	N	N	N	N	N	N
Ecosystem Demography	N	Y	N	N	N	Y[c]	N	N	N
Dynamic natural PFT coverage	Y	Y	Y	N					
Processes relevant to ELUC									
Wood Harvest	Y	Y	Y	Y	Y	N	Y	Y	N
Shifting Cultivation/Subgrid transitions	Y	Y	N	N	N	N	Y	N	N
Crop harvest	Y	Y	Y	Y	Y	Y	Y	Y	Y
Peat fires	N	N	N	N	N	N	N	N	N
Tillage	N	Y	N	N	Y	N	N	N	N
Irrigation	N	Y	N	N	N	N	N	N	N

[a]Available but not provided to TRENDY. [b]Very rudimentary, represents some aspects of N Limitation on photosynthesis driven by soil processes. [c]Basic representation of demography (yearly cohorts, self thinning).

2.1.6. Additional Data Sets

Each DGVM is free to use its own data sources for vegetation and soil types, soil textural properties, soil permeable depth and topography data (e.g., to simulate lateral water flows and soil erosion) as well as for the land mask. Additional data are required for fire-enabled DGVMs including, for example, spatio-temporal maps of lightning ignition and population density, the latter used to estimate human impacts on wildfire regimes. Given the uncertainty around lightning data sets (Kaplan & Lau, 2021), scaling factors, for example, proportion of cloud-cloud versus cloud-ground strikes, and potential need for model recalibration, and the fact that in TRENDY we want models to supply their best C-cycle representation, modeling groups are free to choose their lightning data set. Gridded population density is based on HYDE3.3.

2.2. Models

Seventeen DGVMs participated in TRENDY-v11 (Table 1, Table S2 in Supporting Information S1). While DGVMs are process-based, bottom-up models, the processes included, and their parameterizations vary across

19449224, 2024, 7, Downloaded from https://agupubs.onlinelibrary.wiley.com/doi/10.1029/2024GB008102 by University Of Illinois At, Wiley Online Library on [22/07/2024]. See the Terms and Conditions (https://onlinelibrary.wiley.com/terms-and-conditions) on Wiley Online Library for rules of use; OA articles are governed by the applicable Creative Commons License

Table 2
Factorial Dynamic Global Vegetation Model Simulations With Varying (Observed Historical Evolution), Pre-Industrial (Constant) Forcing for Environmental Conditions (Climate, Atmospheric CO_2 Concentrations, Nitrogen Deposition and Fertilizer Application, Land Use and Land Cover Changes)

	$[CO_2]$	Ndeposition	Nfertilizer	Climate	LULCC	Purpose
S0	Pre-Ind.	Pre-Ind.	Pre-Ind.	Pre-Ind.	Pre-Ind.	Identify model drift
S1	Varying	Varying	Pre-Ind.	Pre-Ind.	Pre-Ind.	CO_2 fertilization effect
S2	Varying	Varying	Pre-Ind.	Varying	Pre-Ind.	SLAND, Nat. Land Sink
S3	Varying	Varying	Varying	Varying	Varying	S2–S3: E_{LUC} under transient env.

models. The key biological and land-use processes included in the individual DGVMs are listed in Table 1 (adapted from Table A1 in Friedlingstein et al. (2022a)). DGVMs run at a spatial resolution: 0.5 × 0.5 (longitude × latitude) degrees (or at a coarser resolution if necessary; ideally at 0.5°).

2.3. Factorial Simulations and Protocol

Initially all DGVMs conduct a spin-up with CO_2 and land cover at their year 1700 levels. While models are free to choose their land cover (typically consisting of the plant functional types they represent) the crop and pasture area distribution correspond to the year 1700. Some DGVMs further use 1700 harvest from LUH2 (Table 1). The CO_2 concentration is set to 276.59 ppm. In the absence of pre-industrial climate data, the climate data from the years 1901–1920 are used repeatedly until model pools reach equilibrium. Whether the climate data is cycled or randomly drawn is thereby model dependent. Subsequently to the spin-up, DGVMs perform four factorial simulations, S0-S3, from 1700 to 2021, as follows, and summarized in Table 2:

S0: A control pre-industrial simulation in which all forcings stay as in the spin-up. S0 allows to diagnose any "cold start" issues and model drift.
S1: In this simulation observed global CO_2 evolves over the historical period, the climate and land cover forcings stay at their pre-industrial levels like in simulation S0. Note: some models also use transient N deposition rates and/or population data in this simulation (see below).
S2: In this simulation, CO_2 and climate evolve over the historical period, while the land cover stays at its pre-industrial level. For the period 1700–1920, the climate data from 1901 to 1920 is used repeatedly and from 1921 to 2021 the climate data for the corresponding years is used.
S3: All forcings (CO_2, climate and land use) evolve over the historical period in this simulation. The meteorological data is used in the same way as in the S2 simulation.

These runs are used for attribution of changes in model's state variables and fluxes to the three global change drivers (CO_2, climate change, and land use change) (Table 2). The S1 simulation mainly quantifies the effect of the anthropogenically increased CO_2 (Walker et al., 2020) but for some models also secondary effects following increases in N deposition and changes in fire dynamics following population increases (see below). The difference between S2 and S1 simulations quantifies the impact of climate variability and change, and the difference between S3 and S2 simulations yields the impact of land-use and land cover change on the evolution of the land carbon sink. Since the S2 simulation uses land-cover corresponding to the pre-industrial state (year 1700), the environmental change effects (CO_2, climate) act on a larger area of natural land than in reality, that is, those areas affected by land-use change since the pre-industrial period. Thus, the simulated land sink (S_{LAND}) in the S2 simulation is likely overestimated globally given the net conversion of natural vegetation (e.g., forests) to agriculture, where the latter has faster carbon turnover times and a smaller sink potential. This process was first termed the land-use amplifier (Gitz & Ciais, 2003; Sitch et al., 2005), and more recently the "Loss of Additional Sink Capacity" (LASC) (Gasser & Ciais, 2013; Pongratz et al., 2014). Thus, DGVM land-use and land cover change emissions (E_{LUC}) derived from differencing S3 and S2 simulations, implicitly include this LASC term, which is substantial and accounts for ∼40% of the present-day DGVM E_{LUC} (Obermeier et al., 2021). This estimate was based on additional DGVM factorial simulations in TRENDY-v8 (GCB2019) to estimate E_{LUC} under pre-industrial and present-day environmental conditions, and thus used to diagnose the LASC (Obermeier et al., 2021). The inclusion of the LASC complicates comparison of E_{LUC} estimates from DGVMs with other methodologies (e.g., bookkeeping and NGHGIs) which do not take LASC into account.

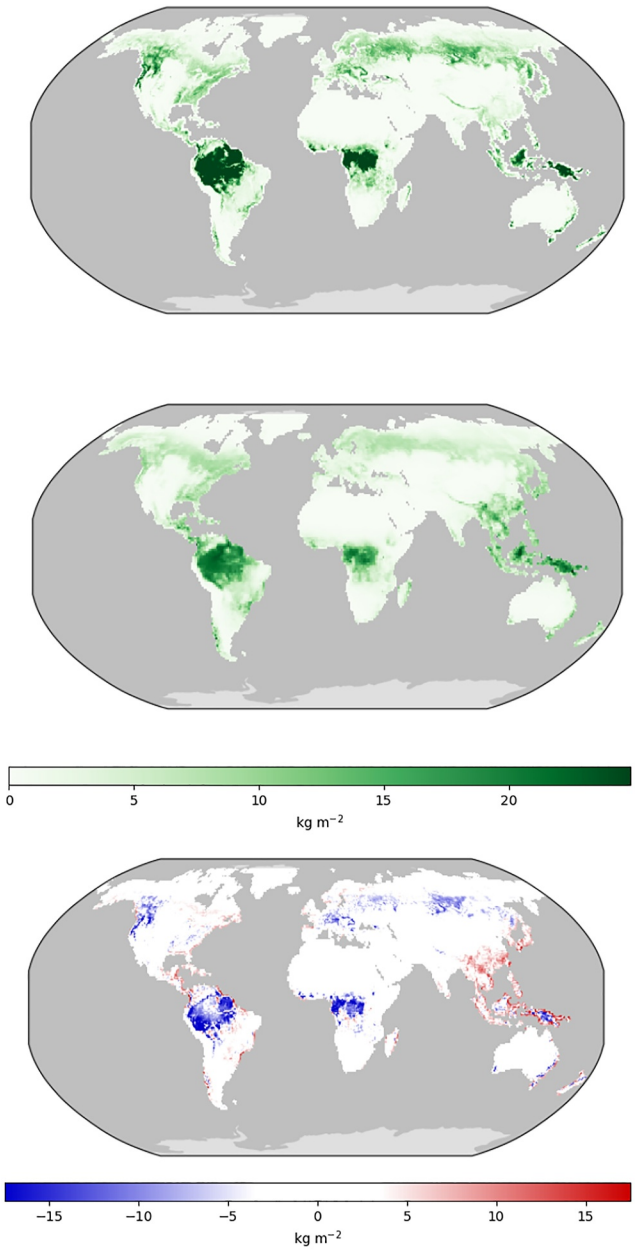


Figure 4. Biomass benchmark data sets. (a) ESA CCI v3 2010. (b) Multi-Model Ensemble Mean biomass. (c) difference (MMEM—ESA CCI).

In addition to the forcings described above, models that include a representation of the terrestrial nitrogen cycle (see Table 1) require pre-industrial or time varying N deposition and N fertilizer application rates as follows:

S0: This simulation uses N deposition and fertilizer application rates corresponding to their pre-industrial level (year 1700).
S1: Time varying N deposition rates but pre-industrial N fertilizer application rates are used.
S2: Time varying N deposition rates but pre-industrial N fertilizer application rates are used
S3: Time varying N deposition and N fertilizer application rates are used.

DGVMs that represent fire use time-evolving population density, itself linked to fire ignition and suppression, in simulations S1-S3, and population density for the year 1700 in simulation S0. Our simplified logic is that LULCC and its direct consequences (Nfert) go together in E_{LUC}, and all other indirect environmental changes (Ndep, population, climate, CO_2) in S_{LAND}.

2.4. Criteria for Budget Inclusion

DGVMs are included in GCB assessments if they fulfill a set of three criteria for minimum model realism:

1. Steady state after spin-up. Steady-State defined as an offset of global NBP <0.10 PgC/yr, drift <0.05 PgC/yr per century (i.e., first is the average over 1700–2021, second is the NBP ∼ year slope × 100). Diagnosed from S0 run.
2. The global net annual land flux (S_{LAND}−E_{LUC}) is a carbon sink over the 1990s and 2000s as constrained by global atmospheric and oceanic observations (Keeling & Manning, 2014). Diagnosed from S3 run.
3. Global net annual land use flux (E_{LUC}) is a carbon source over the 1990s, based on results of book-keeping models (IPCC, 2007). Diagnosed from S3–S2 runs.

2.5. Benchmarking

DGVMs are evaluated and compared in the ILAMB benchmarking system and summary statistics given for each model (in summary table/figures in the supplementary material of the annual GCB assessments). This allows to document model improvement each year, and to identify possible issues/model deficiencies to aid model development. We currently do not use the benchmarking results as criteria for budget inclusion or model weighting, but rather to encourage modeling groups to continue to improve their models. In future years and with consultation among participating groups, benchmarking could play a role in model inclusion or weighting. The selection of tests, metrics and performance criteria are subjective, and observation-based data uncertainty would further need to be included (Seiler et al., 2022). A medium-term objective will be to use benchmarking to weight model performance for the Multi-Model Ensemble Mean (MMEM), with aim to help reduce the Budget Imbalance, which is the remaining unexplained uncertainty in the global carbon budget.

2.6. Outputs

For GCB assessments four aggregated NBP values (PgC/yr) are requested from all simulations (S0 to S3): annual global NBP, annual northern extra tropics NBP (>30°N), annual tropical NBP (30°S < latitude < 30°N) annual southern extra-tropics NBP (<30°S); for the years 1700–2021.

19449224, 2024, 7, Downloaded from https://agupubs.onlinelibrary.wiley.com/doi/10.1029/2024GB008102 by University Of Illinois At, Wiley Online Library on [22/07/2024]. See the Terms and Conditions (https://onlinelibrary.wiley.com/terms-and-conditions) on Wiley Online Library for rules of use; OA articles are governed by the applicable Creative Commons License

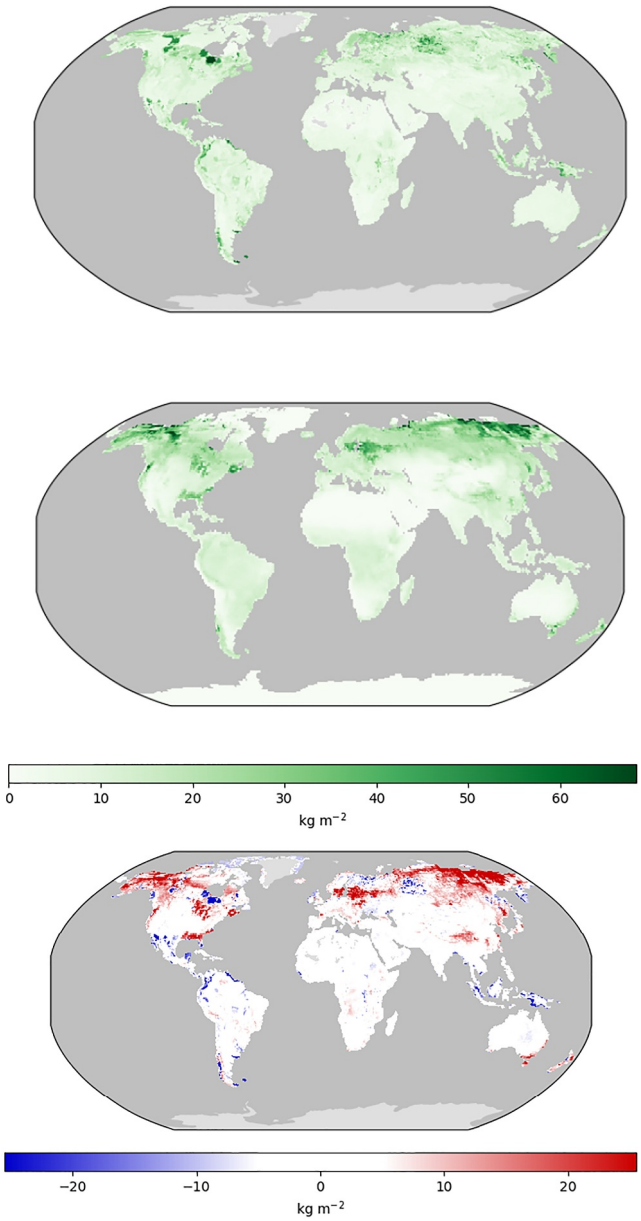


Figure 5. Soil Carbon benchmark. (a) HWSDvn1.2. (b) Multi-Model Ensemble Mean C soil. (c) difference (MMEM—HWSD), all for year 2000.

An extended list of gridded output variables for carbon and water cycling, and energy balance is requested (see Tables S3–S6 of Supporting Information S1), which are then available to the research community for spin-off studies. Variables are listed as either, Level 1: essential, which all DGVM groups are strongly encouraged to deliver, and Level 2 variables: as desirable for additional in-depth analysis/studies. To enable alignment with national inventories we need DGVMs to output NBP on a Plant Functional Type basis where possible (Grassi et al., 2018). This is to separate fluxes on managed versus unmanaged land.

3. Results

3.1. Benchmarking Carbon and Hydrological Cycles

In GCB we provide a summary benchmarking table for the key carbon and hydrological cycle variables. An exhaustive benchmarking analysis has been performed by Seiler et al., 2022 on the earlier TRENDY-v9 with focus on uncertainty in models and observation-based data sets. We do not expect major differences in results and therefore give a broad overview of model performance for a small set of key carbon stocks and fluxes: biomass, soil carbon, and GPP; and water cycle variables: river runoff and evapotranspiration. In TRENDY, DGVMs have been evaluated within the ILAMB benchmarking tool (Collier et al., 2018).

Here we summarize the model-data evaluation for the S3 simulation, and the full suite of TRENDY ILAMB benchmarking results can be accessed below, which updated each GCB cycle provides an essential service to the modeling community: https://gws-access.jasmin.ac.uk/public/jules/TRENDY2022/GCP_220523_vn2.6_global/.

Using four regional and global biomass data sets (Santoro & Cartus, 2021; Saatchi et al., 2011; Thurner et al., 2014; GlobalCarbon unpublished data) the MMEM performance is in reasonable agreement, in terms of spatial variation in biomass across biomes. The MMEM tends to under-estimate biomass against the ESA-CCI benchmark year 2010 (Figure 4) but overestimate the GlobalCarbon benchmark (see ILAMB link), despite the ESA-CCI benchmark only estimating aboveground biomass, while the other benchmarks estimate total biomass. This highlights how uncertainty across observation-based products needs to be considered in benchmarking analyses (Seiler et al., 2022). Against the regional biomass data sets, the MMEM overestimates biomass in the tropics, and in the boreal and tundra regions, and underestimates biomass in mid-latitude northern and temperate regions. H. Yang et al. (2023) suggests DGVMs may overestimate biomass in tropical forests in the absence of forest degradation processes (e.g., through selective logging and forest fires).

The ensemble performs well for soil carbon against the one global soil carbon data set (HWSD, Wieder, Boehnert, & Bonan, 2014; Wieder, Boehnert, Bonan, & Langseth, 2014; Figure 5), albeit overestimating in high latitudes, in Alaska and Siberia, against both the global and regional (see ILAMB link) benchmark data sets. Two DGVMs simulate very high soil stocks in the high northern latitudes. However, a note of caution, a second global soil database (https://soilgrids.org) also has higher soil C stocks in high latitudes.

DGVMs generally perform well against fluxnet-derived and FLUXCOM GPP for spatial variance over 1980–2014 (Figure 6), although the benchmark data are biased toward mid-latitude sites. The MMEM slightly underestimates the data-derived peak in amplitude in the seasonal cycle of GPP (not shown - see ILAMB link).

DGVMs perform very well in simulating spatial patterns of river runoff (Figure 7), particularly its interannual variability (see ILAMB link), however, tend to underestimate runoff in major river basins, for example, the

19449224, 2024, 7, Downloaded from https://agupubs.onlinelibrary.wiley.com/doi/10.1029/2024GB008102 by University Of Illinois At, Wiley Online Library on [22/07/2024]. See the Terms and Conditions (https://onlinelibrary.wiley.com/terms-and-conditions) on Wiley Online Library for rules of use; OA articles are governed by the applicable Creative Commons License

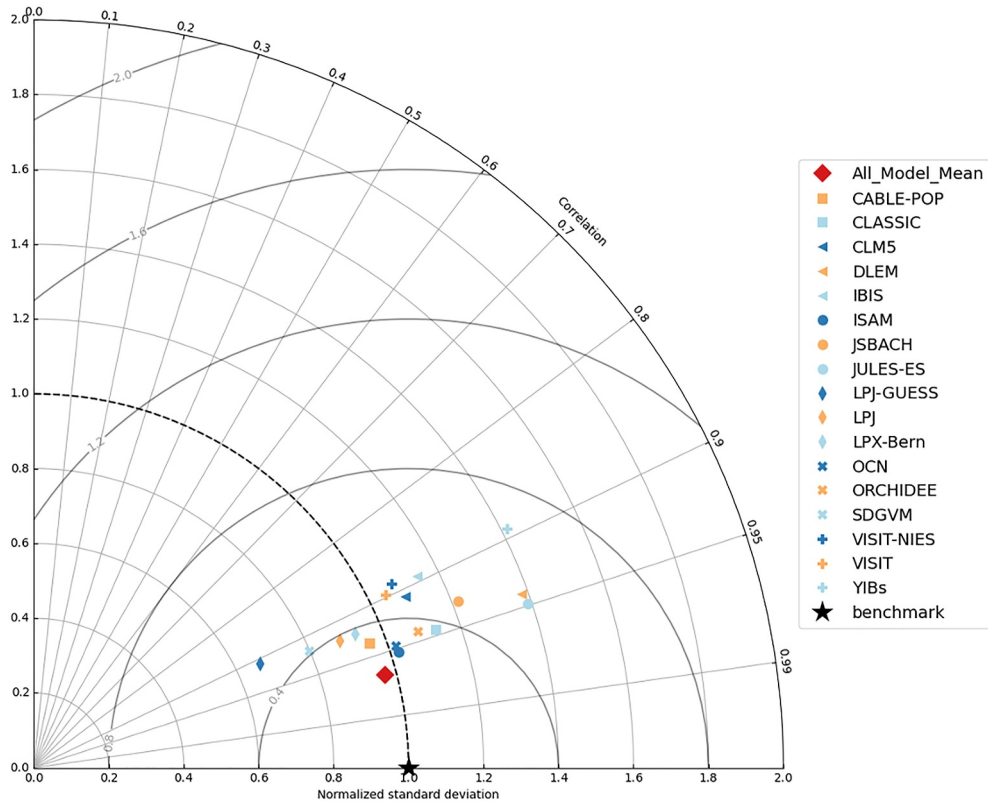


Figure 6. Taylor diagram comparing the spatial distribution of GPP against the FLUXCOM data set (Jung et al., 2017; Tramontana et al., 2016). Compares time-means over the period 1980–2014.

Amazon, and in S.E. Asia, possibly due to the lack of lateral flow processes and river routing in most models. DGVMs also perform well against GLEAM evapotranspiration product, in particular the seasonal cycle (see ILAMB link). ILAMB also allows the evaluation of relationships between variables, for example, GPP versus ET (Figure 8), which is also available for each of the 10 main RECCAP2 regions (*see* 10 regional and global options under *Global-Land*): https://gws-access.jasmin.ac.uk/public/jules/TRENDY2022/GCP_220523_vn2.6/.

3.2. Spatio-Temporal Changes in NBP, Drivers, and Process Attribution

3.2.1. Global NBP and Environmental Drivers

The long-term evolution of the net land-atmosphere exchange and the attribution to individual drivers is shown in Figure 9. Since the 1950s, rising atmospheric CO_2 concentrations have increased carbon uptake to an average of 3.8 ± 0.8 PgC/yr over 2012–2021. The natural land sink is reduced by the effects of climate variability and change (-0.6 PgC/yr $\pm$ 0.5 PgC/yr). Over the same period, E_{LUC} has remained roughly constant (-1.6 ± 0.5 PgC/yr). Hence, the land is a net sink of carbon globally (1.7 ± 0.6 PgC/yr) over the 2012–2021 period. On inter-annual timescales, climate impacts global land carbon fluxes primarily via ENSO variability (Keeling et al., 1995; Peylin et al., 2005; Piao et al., 2019; Tian et al., 1998).

3.2.2. NBP and Process Attribution

In recent decades, the simulated net land-atmosphere exchange is mainly driven by the CO_2 response of photosynthesis and biomass production (Walker et al., 2020; Figures 9, 10i, 10j, and 11). Further, increased nitrogen deposition may have also contributed to enhanced plant growth (Townsend et al., 1996). The models simulate a small reduction in global burnt area over 2012–2021 (Figure S2 in Supporting Information S1), in agreement with satellite-based data sets, which attribute changes primarily to cropland expansion and its intensification (Andela et al., 2017). However, the ability of recent high-resolution remote-sensing to detect widespread small fires cautions the validity of trends based on earlier coarse-resolution products (Chuvieco

19449224, 2024, 7, Downloaded from https://agupubs.onlinelibrary.wiley.com/doi/10.1029/2024GB008102 by University Of Illinois At, Wiley Online Library on [22/07/2024]. See the Terms and Conditions (https://onlinelibrary.wiley.com/terms-and-conditions) on Wiley Online Library for rules of use; OA articles are governed by the applicable Creative Commons License

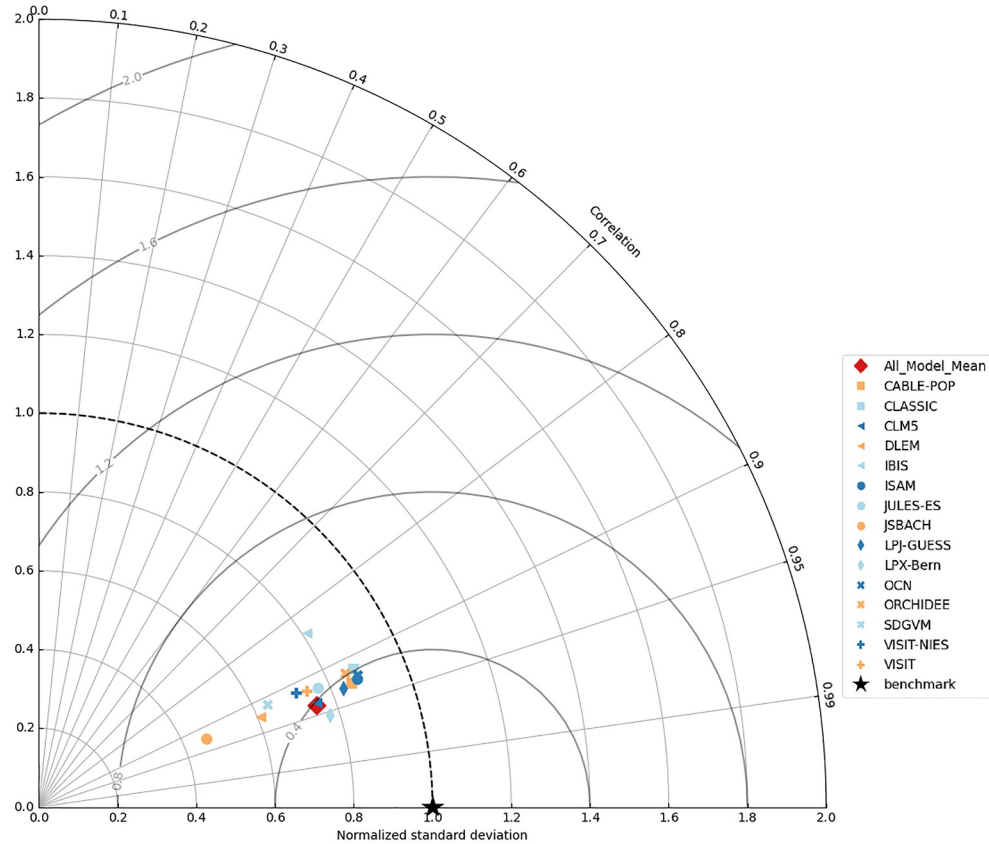


Figure 7. Taylor diagram evaluating the spatial distribution of river runoff (Dai & Trenberth, 2002). Time-mean basin runoff is used from the period 1980–2011.

et al., 2022; Ramo et al., 2021). LULCC has reduced global fire emissions by ∼0.3 PgC/yr compared to the start of the 20th century. The specific contribution of recent changes in climate-alone act to increase fire risk and increase global burnt area since around 1980 (Jones et al., 2022), but have a small impact on simulated carbon emissions (Figure S2 in Supporting Information S1). Indeed, while carbon emissions from fires have reduced in savannahs and increased in forests and approximately balanced globally (Zheng et al., 2021). There is no clear consensus as to how rising CO_2 concentrations influence global burnt area, but CO_2-induced gains in biomass stocks lead to

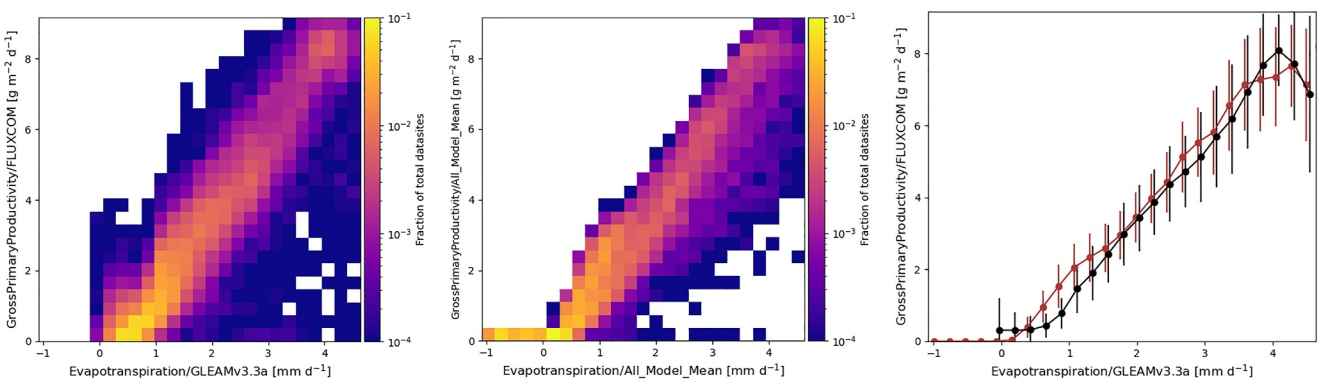


Figure 8. Relationships between variables from the benchmark data sets (a) GPP Fluxcom versus ET GLEAM (b) GPP versus ET Multi-Model Ensemble Mean (MMEM) (c) data-derived (black) versus MMEM (brown) relationship between GPP and ET. Colors on (a) and (b) indicate the fraction of gridboxes in each bin. Error bars on (c) indicate ±1 standard deviation of GPP at gridboxes with ET in a given bin.

19449224, 2024, 7, Downloaded from https://agupubs.onlinelibrary.wiley.com/doi/10.1029/2024GB008102 by University Of Illinois At, Wiley Online Library on [22/07/2024]. See the Terms and Conditions (https://onlinelibrary.wiley.com/terms-and-conditions) on Wiley Online Library for rules of use; OA articles are governed by the applicable Creative Commons License

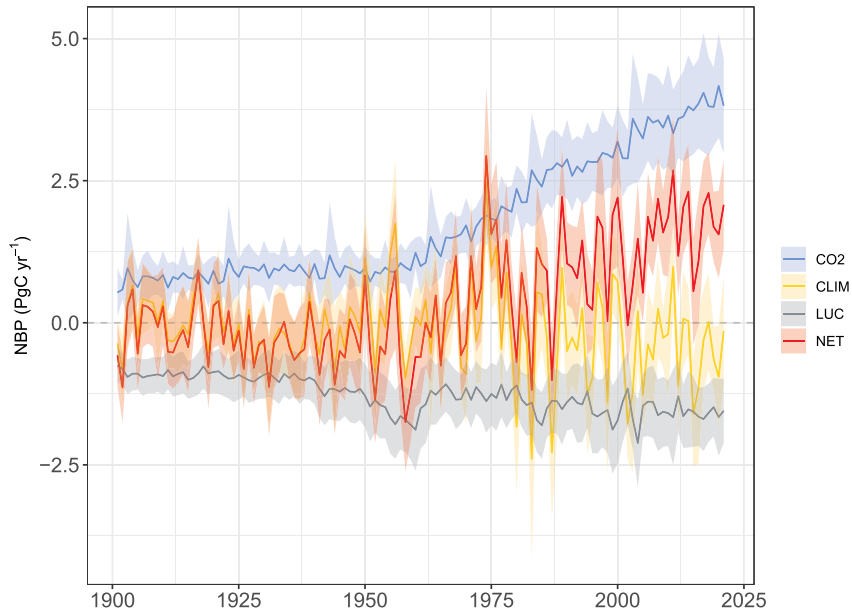


Figure 9. Timeseries of global NBP attributed to processes CO_2, Climate and Land Use and Land Cover Changes and the sum of the three (NET). Shown is the multi-model ensemble mean.

increased fire emissions when vegetation is eventually burned. A more comprehensive assessment of fire-enabled DGVMs has been conducted by FireMIP (Hantson et al., 2016, 2020; Li et al., 2019; Rabin et al., 2017).

3.2.3. Ecosystems Contribution to NBP

Biome contribution to mean, trend, and interannual variability in the natural sink is shown in Figure 12 and how their contributions vary per decade in Figures S3 and S4 of Supporting Information S1. Three biomes (tropical forest, semi-arid and grasslands/crops) are the most important on all three timescales, with the greatest contribution of the semi-arid biome to the interannual variability, as found in Ahlström et al. (2015), Piao et al. (2019), and Poulter et al. (2014). IAV in the carbon cycle is driven by ENSO climate variability, and it is notable that the last decade has been characterized by La Niñas (2011, 2020, 2021), punctuated by one large 2015/16 El Niño, in contrast with an El Niño dominated decade of the 1990s. The IAV contribution does not appear to vary significantly by decade (Figure S3 in Supporting Information S1). The relative biome contribution to the long-term trend also does not change (Figure S4 in Supporting Information S1), except for a decrease in contribution of the tropical forest between 1982 and 2001, and 2002–2021. This may indicate a decline in the tropical intact forest sink strength, which has been observed in forest plot networks (Brienen et al., 2015; Hubau et al., 2020), and broadly attributed to drought-impacts on forest function. DGVMs are likely to underestimate drought impacts, as they lack explicit drought mortality, however, will simulate reductions in GPP with water deficit, albeit only few DGVMs explicitly represent plant hydraulics, a field of active recent development (Eller et al., 2020; S. Wang et al., 2020; Y. Wang et al., 2020).

3.2.4. Regional Contribution to NBP

Regional attribution (RECCAP2-regions) is shown in Figure 13, and in Table 3 for the decades 2000–2009 and 2012–2021. A positive effect of increasing atmospheric CO_2 on the simulated land carbon sink is broadly consistent with empirical understanding and measurements at smaller scales albeit measurement of the CO_2 effect at regional to global scales is not currently possible (Walker et al., 2020). Boreal and temperate regions are simulated to have increased carbon stocks in response to moderate warming, for example, with longer growing seasons and enhanced nutrient cycling and N deposition (Piao et al., 2007), whereas low latitude regions are negatively impacted by climate, suggesting that warming combined with drought reduces plant productivity. The largest LULCC emissions are in the tropical regions over the past decade.

19449224, 2024, 7, Downloaded from https://agupubs.onlinelibrary.wiley.com/doi/10.1029/2024GB008102 by University Of Illinois At, Wiley Online Library on [22/07/2024]. See the Terms and Conditions (https://onlinelibrary.wiley.com/terms-and-conditions) on Wiley Online Library for rules of use; OA articles are governed by the applicable Creative Commons License

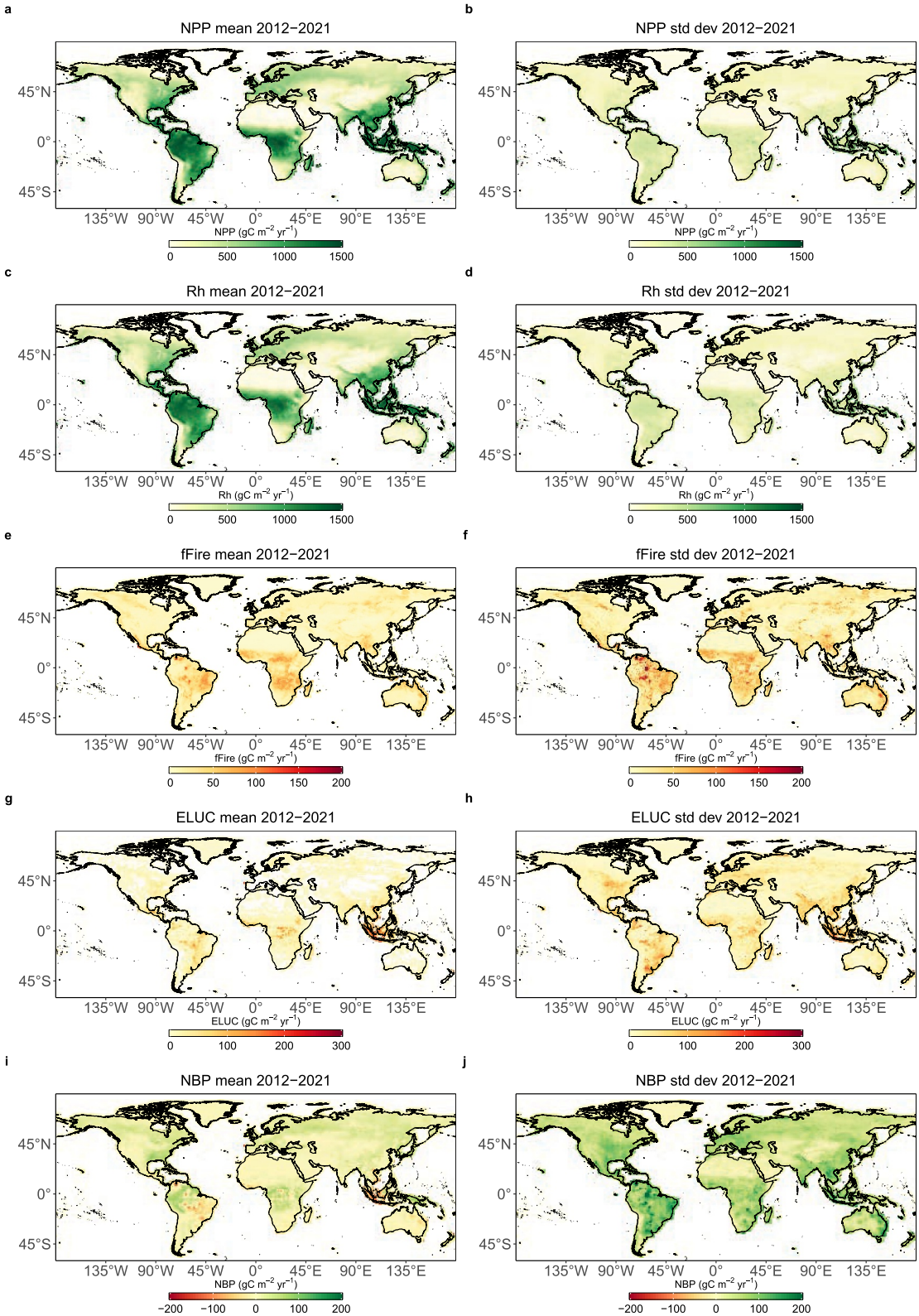


Figure 10. Dynamic Global Vegetation Model Multi-Model Ensemble Mean and 1 standard deviation carbon fluxes for the present-day (2012–2021).

19449224, 2024, 7, Downloaded from https://agupubs.onlinelibrary.wiley.com/doi/10.1029/2024GB008102 by University Of Illinois At, Wiley Online Library on [22/07/2024]. See the Terms and Conditions (https://onlinelibrary.wiley.com/terms-and-conditions) on Wiley Online Library for rules of use; OA articles are governed by the applicable Creative Commons License

19449224, 2024, 7, Downloaded from https://agupubs.onlinelibrary.wiley.com/doi/10.1029/2024GB008102 by University Of Illinois At, Wiley Online Library on [22/07/2024]. See the Terms and Conditions (https://onlinelibrary.wiley.com/terms-and-conditions) on Wiley Online Library for rules of use; OA articles are governed by the applicable Creative Commons License

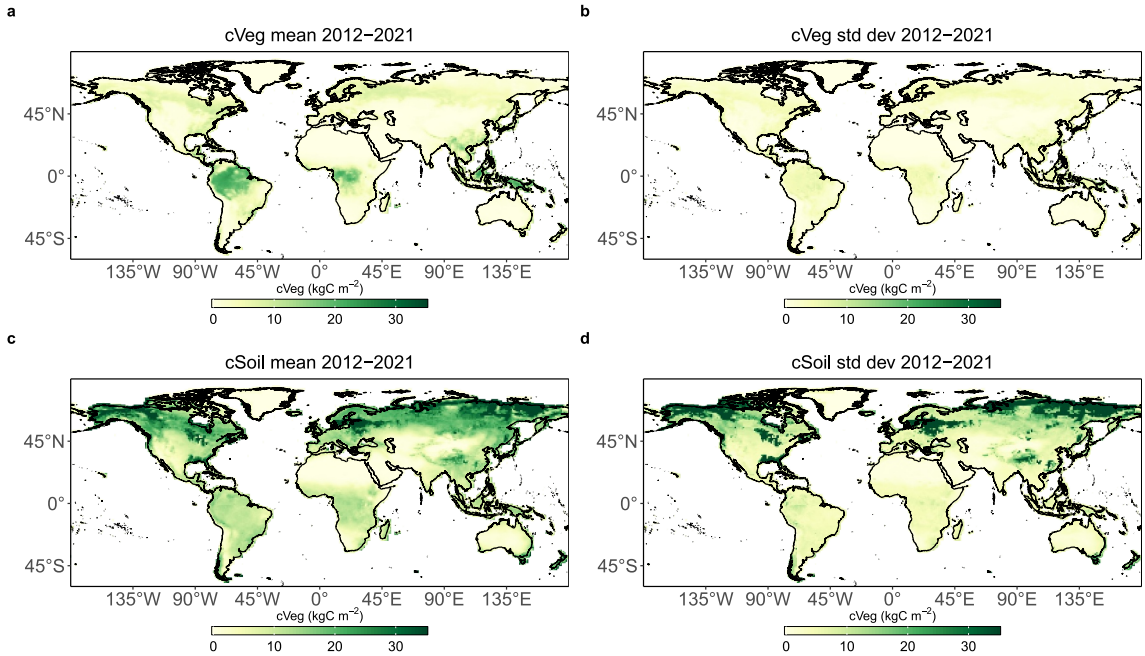


Figure 11. Dynamic Global Vegetation Model Multi-Model Ensemble Mean and 1 standard deviation carbon stocks in vegetation and soils for the present-day (2012–2021).

Land abandonment and preservation, reforestation efforts and improved land management practices particularly in the second half of the 20th century (Nabuurs et al., 2003) led to carbon sinks in regrowing temperate forests, although there is evidence of potential sink saturation and subsequent declines during the 21st century, for example, in Europe (Nabuurs et al., 2013; Winkler et al., 2023). In contrast, DGVMs simulate a LULCC source in mid-latitude regions, which may reflect that forest-age, demography and wood harvest is not properly represented in most DGVMs, and emphasizes the importance of simulating gross transitions. This may lead to an underestimate in the DGVM simulated net land carbon sink in these regions. Russia and North America are simulated to have the largest net land carbon sink with positive effects of elevated CO_2 and climate on carbon sequestration. Typically, the tropical regions experience the largest gross impacts of CO_2, LULCC, and climate, which counterbalance to give a more moderate net land-atmosphere exchange estimate. The budgets estimated by DGVMs reported here can be compared with the corresponding best estimates currently being developed in the RECCAP2 activity.

Although climate variability and change have the smallest impact on the mean land sink in most regions over the 2012–2021 decade it is the most important driver of regional trends in the 21st Century (Figure 14). Model results suggest a small reduction in land sink capacity in tropical South America and South-East Asia, the former driven by negative impacts of climate change offsetting decadal reductions in deforestation. In contrast climate variability and change has the largest positive contribution to the large land sink trend in Africa and North America.

4. Perspectives

TRENDY aims to further develop and apply model benchmarking in the future, aiming to weight modeled NBP by model performance across a range of observational-based benchmarking tests; that will require consideration of uncertainties in the observation data products. Following the findings of O'Sullivan et al. (2022), further internal-cycling variables will be requested and analyzed to better isolate uncertainty and sensitivity in process representations among DGVMs. These variables include plant allocation and turnover to and from individual tissue pools, and input and loss from individual litter and soils pools, and separate C fluxes associated with individual disturbance agents (e.g., fire, drought and background mortality). Further efforts are needed to reduce the large uncertainty in the CO_2 fertilization effect across DGVMs (Chen et al., 2022; Haverd et al., 2020; Huntingford & Oliver, 2021; Medlyn et al., 2015); empirical efforts with Free-Air-Carbon Dioxide Enrichment experiments in mature temperate forest (BiFOR) and soon the Amazon forest (AmazonFACE) promise large

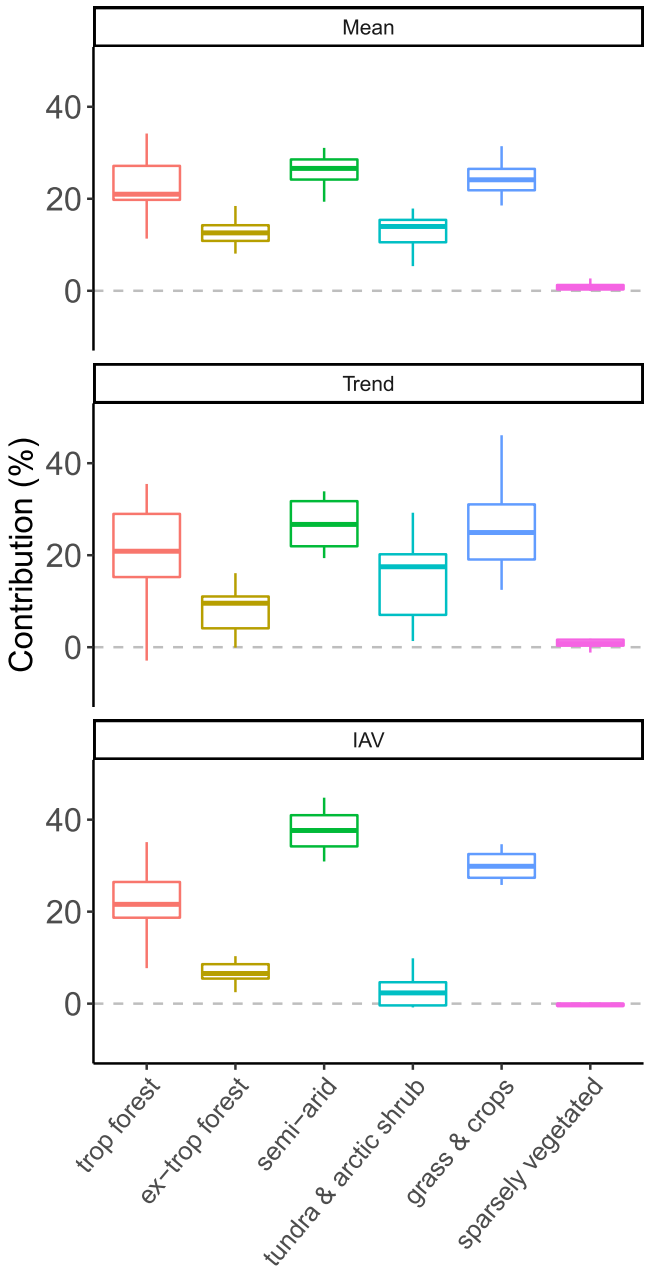


Figure 12. Decomposition of natural land sink into mean, trend, and interannual variability for different biomes, following Ahlström et al. (2015) over the period 1982–2021. Box-plots show Multi-Model Ensemble Mean, interquartile range, and range.

knowledge gains and data sets to constrain DGVMs. DGVM benchmarking is of crucial importance. Modelers need to actively engage with data set providers to understand the most appropriate data sets to include in the benchmarking exercise and discuss how to interpret uncertainty in these products. In TRENDY, DGVMs are forced with one climate data set (CRUJRA) and one land use change reconstruction. Studies with single DGVMs or other types of carbon cycle/book-keeping models have quantified the uncertainty in land carbon cycle variables related to alternative climate forcing data sets (Hardouin et al., 2022; Wu et al., 2017) and land-use data sets (Bayer et al., 2017, 2021; Ganzenmüller et al., 2022), and found that these can be large (Hartung et al., 2021). A systematic assessment using multiple climate forcing data sets is needed across the range of TRENDY models to quantify the impact of climate forcing uncertainty. Many DGVMs (including those coupled within host Earth System Models) contribute to other MIP activities, such as ISIMIP/CMIP-land simulations (e.g., Hardouin et al., 2022), CMIP ESM simulations, the N2O Model Intercomparison (NMIP, Tian et al., 2018, 2019) and FireMIP (Rabin et al., 2017). So, improved benchmarking under TRENDY (a) helps to constrain these other assessments including future climate change work, (b) helps to direct model development that feeds into CMIP7, and (c) supports protocol and forcing data sharing among multiple assessments to improve comparability and reduce modeling teams workload when contributing to more than one assessment, for example, GCP-C (Friedlingstein et al., 2022a), GCP-CH_4 (Saunois et al., 2020) GCP-N_2O (Tian et al., 2020).

Few DGVMs represent ecosystem demography and climate-stress induced mortality, and they vary widely in which land management practices (like wood harvesting, tillage, irrigation) are considered. There is currently a large uncertainty in simulated biomass and its change between DGVMs (H. Yang et al., 2020). Remote-sensing offers great potential to better constrain and calibrate models for biomass, disturbance effects, regrowth and recovery in different forest types (Heinrich et al., 2021, 2023). These will be key processes for model development to robustly represent the impact of climate change and extremes on the land sink (e.g., response to and recovery from heat extremes, drought, and fire), and the impact of land management, on the near-term evolution of the land sink and on land-use fluxes. This information is key to the periodic UNFCCC Global Stocktakes and to inform the remaining human emissions to avoid dangerous climate change. Additionally, TRENDY model outputs have been extensively used to assess retrospectively the impacts of extreme events or other events of interest, for example, El Niño events (Bastos et al., 2018). These typically lag the events of interest by several months if not years. A new initiative is to conduct fast-track assessments of the impact of regional climate extremes and megafires on the carbon cycle in near real time. A new protocol based on Bastos et al. (2020) is currently being developed to complement annual TRENDY, whereby DGVMs are run at set points during a given year (or when required), with forcing updated from ERA5 reanalysis (Hersbach et al., 2020), with an assessment latency of ∼3 months. DGVMs will be applied for an "S2"- style (CO_2 and Climate only, with fixed present-day LUC) simulation, and can be restarted from the end of the previous simulation (to avoid computationally expensive simulations). The additional S2 simulation with ERA5 can also be contrasted with the DGVM simulation with CRUJRA to quantify the impact of climate-driven uncertainty, although the protocols differ considerably.

Rosan et al. (2021) demonstrated the benefit of adopting country-specific LULCC data sets and expertise, particularly those based on low latency, spatio-temporal Earth Observation data. We envisage extending this approach, first for those countries with the largest contribution to ELUC and eventually all countries. There are

19449224, 2024, 7, Downloaded from https://agupubs.onlinelibrary.wiley.com/doi/10.1029/2024GB008102 by University Of Illinois At, Wiley Online Library on [22/07/2024]. See the Terms and Conditions (https://onlinelibrary.wiley.com/terms-and-conditions) on Wiley Online Library for rules of use; OA articles are governed by the applicable Creative Commons License

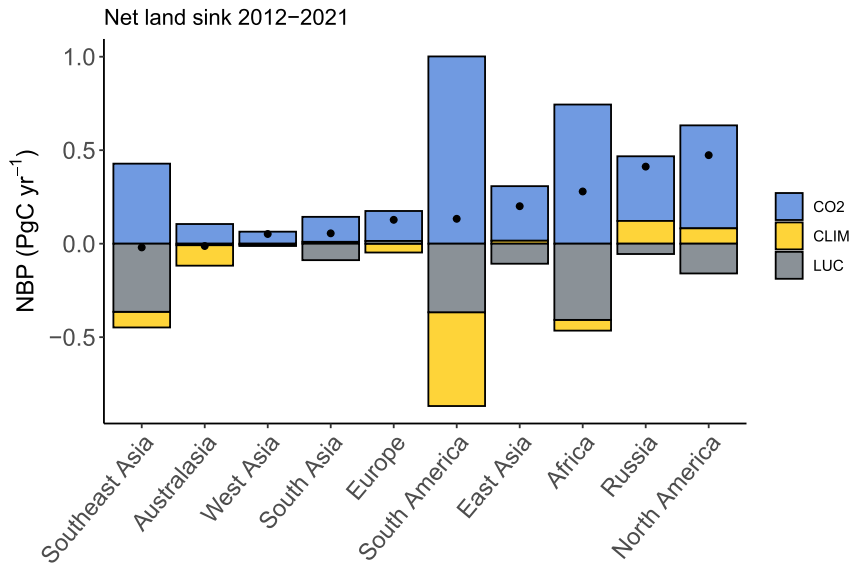


Figure 13. Regional mean net land-atmosphere exchange (symbols) and process attribution (bars) for the 10 main RECCAP2 land regions over 2012–2021.

recognized issues relating to the LULCC data used for China (X. Wang et al., 2024; Yu et al., 2022) and this represents a major uncertainty in GCB. This in part relates to changing methodologies in reporting agricultural areas to FAO through time (Yu et al., 2022). We aim to adopt these alternative data sets in the future.

A final medium-term objective is to combine the land GHG budgets for CO_2, CH_4, and N_2O in near-real-time assessments, for example, to contribute to initiatives like the WMO for a GHG monitoring system (WMO, 2023).

5. Summary

The TRENDY project has completed its 11th annual iteration and delivered natural land sink and land-use emission estimates to the GCP-Global Carbon Budget 2022. The project has served the global land modeling community for over a decade, providing a forum to evaluate, intercompare and guide future model development, and its data have been used in over 100 peer-reviewed publications (https://blogs.exeter.ac.uk/trendy/publications/) to enhance our understanding of land biogeochemical cycles. In this study we have described the latest TRENDY project protocols and input data sets and provided summary information on the terrestrial carbon cycle

Table 3
Decadal NBP (±1 Standard Deviation) in PgC/yr and Their Process Attribution for 2000–2009 and 2012–2021 for Ten RECCAP2 Land Regions

	2000–2009				2012–2021			
Regions	CO_2	Climate	LULCC	Net	CO_2	Climate	LULCC	Net
North America	0.51 ± 0.17	−0.02 ± 0.13	−0.16 ± 0.09	0.33 ± 0.14	0.55 ± 0.17	0.08 ± 0.17	−0.16 ± 0.09	0.47 ± 0.21
South America	0.84 ± 0.18	−0.16 ± 0.14	−0.49 ± 0.22	0.19 ± 0.15	1 ± 0.24	−0.5 ± 0.24	−0.37 ± 0.17	0.13 ± 0.19
Europe	0.13 ± 0.05	0 ± 0.06	0.01 ± 0.04	0.14 ± 0.06	0.16 ± 0.06	−0.05 ± 0.07	0.01 ± 0.05	0.13 ± 0.07
Africa	0.65 ± 0.16	−0.2 ± 0.15	−0.36 ± 0.16	0.08 ± 0.17	0.74 ± 0.19	−0.06 ± 0.12	−0.41 ± 0.17	0.28 ± 0.16
Russia	0.31 ± 0.13	0.15 ± 0.19	−0.04 ± 0.06	0.41 ± 0.24	0.35 ± 0.16	0.12 ± 0.19	−0.06 ± 0.06	0.41 ± 0.27
West Asia	0.06 ± 0.04	−0.01 ± 0.04	−0.01 ± 0.01	0.04 ± 0.03	0.06 ± 0.03	−0.01 ± 0.02	0 ± 0.01	0.05 ± 0.03
East Asia	0.26 ± 0.06	−0.07 ± 0.08	−0.08 ± 0.1	0.11 ± 0.1	0.29 ± 0.06	0.02 ± 0.08	−0.11 ± 0.09	0.2 ± 0.13
South Asia	0.1 ± 0.04	−0.04 ± 0.03	−0.05 ± 0.05	0.02 ± 0.05	0.13 ± 0.04	0.01 ± 0.03	−0.09 ± 0.07	0.06 ± 0.06
Southeast Asia	0.38 ± 0.16	−0.02 ± 0.05	−0.34 ± 0.13	0.02 ± 0.09	0.43 ± 0.2	−0.08 ± 0.08	−0.36 ± 0.14	−0.02 ± 0.08
Australasia	0.09 ± 0.03	−0.09 ± 0.06	−0.01 ± 0.03	−0.01 ± 0.06	0.11 ± 0.04	−0.11 ± 0.06	−0.01 ± 0.02	−0.01 ± 0.07
Global	3.33 ± 0.66	−0.47 ± 0.52	−1.54 ± 0.59	1.33 ± 0.57	3.83 ± 0.77	−0.58 ± 0.54	−1.55 ± 0.51	1.7 ± 0.6

19449224, 2024, 7, Downloaded from https://agupubs.onlinelibrary.wiley.com/doi/10.1029/2024GB008102 by University Of Illinois At, Wiley Online Library on [22/07/2024]. See the Terms and Conditions (https://onlinelibrary.wiley.com/terms-and-conditions) on Wiley Online Library for rules of use; OA articles are governed by the applicable Creative Commons License

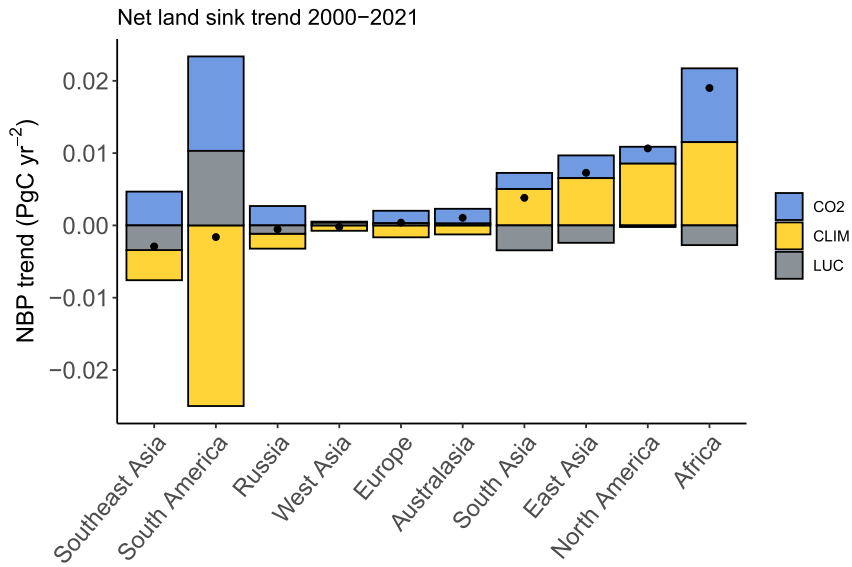


Figure 14. Trends in the net exchange over the 21st Century (2000–2021) and underlying process attribution.

across large regions and their process attribution, and individual model performance across a range of benchmarking tests. The largest gross fluxes are simulated in the tropical regions, with the negative effects of land-use change, through deforestation, plus a small negative contribution of climate variability and change, that counteract simulated positive effects of CO_2 fertilization on the net land-atmosphere exchange. In contrast, in extratropical regions CO_2 fertilization dominates and is supplemented by a small positive effect of climate change, extending high-latitude growing seasons, with a smaller contribution of land-use change on the net land-atmosphere exchange.

Data Availability Statement

All TRENDY-v11 data are freely available from the following website: https://globalcarbonbudgetdata.org/.

Acknowledgments

This work is part of the GCP-RECCAP2 project which is supported by the ESA Climate Change Initiative (contract no. 4000123002/18/I-NB), ESA Carbon-RO (4000140982/23/I-EF), European Union's Horizon 2020 research and innovation program under Grant Agreement No. 821003 (project 4C), the UK's Natural Environment Research Council (NE/S015833/1), and the CALIPSO (Carbon Losses in Plants, Soils and Oceans) project, funded through the generosity of Eric and Wendy Schmidt by recommendation of the Schmidt Futures program. H.T. acknowledges funding support from the U.S. National Science Foundation (Grant numbers: 1903722). JGC acknowledges funding from the Australian National Environmental Science Program - Climate Systems Hub. ORNL is managed by UT-Battelle, LLC, for the DOE under contract DE-AC05-1008 00OR22725. E.R. was supported by the Newton Fund through the Met Office Climate Science for Service Partnership Brazil (CSSP Brazil) and by the Met Office Hadley Centre Climate Programme funded by BEIS. For the purpose of open access, the author has applied a "Creative Commons Attribution (CC BY) license to any Author Accepted Manuscript version arising."

References

Ahlström, A., Raupach, M. R., Schurgers, G., Smith, B., Arneth, A., Jung, M., et al. (2015). The dominant role of semi-arid ecosystems in the trend and variability of the land CO_2 sink. *Science*, *348*(6237), 895–899. https://doi.org/10.1126/science.aaa1668

Andela, N., Morton, D. C., Giglio, L., Chen, Y., van der Werf, G., Kasibhatla, P. S., et al. (2017). A human-driven decline in global burned area. *Science*, *356*(6345), 1356–1362. https://doi.org/10.1126/science.aal41

Arneth, A., Sitch, S., Pongratz, J., Stocker, B. D., Ciais, P., Poulter, B., et al. (2017). Historical carbon dioxide emissions caused by land-use changes are possibly larger than assumed. *Nature Geoscience*, *10*(2), 79–84. https://doi.org/10.1038/ngeo2882

Arora, V. K., Katavouta, A., Williams, R. G., Jones, C. D., Brovkin, V., Friedlingstein, P., et al. (2020). Carbon–concentration and carbon–climate feedbacks in CMIP6 models and their comparison to CMIP5 models. *Biogeosciences*, *17*(16), 4173–4222. https://doi.org/10.5194/bg-17-4173-2020

Bastos, A., Friedlingstein, P., Sitch, S., Chen, C., Mialon, A., Wigneron, J.-P., et al. (2018). Impact of the 2015/2016 El Niño on the terrestrial carbon cycle constrained by bottom-up and top-down approaches. *Philosophical Transactions of the Royal Society of London B Biological Sciences*, *373*(1760), 20170304. https://doi.org/10.1098/rstb.2017.0304

Bastos, A., O'Sullivan, M., Ciais, P., Makowski, D., Sitch, S., Friedlingstein, P., et al. (2020). Sources of uncertainty in regional and global terrestrial CO_2 exchange estimates. *Global Biogeochemical Cycles*, *34*(2), e2019GB006393. https://doi.org/10.1029/2019gb006393

Bayer, A. D., Fuchs, R., Mey, R., Krause, A., Verburg, P. H., Anthoni, P., & Arneth, A. (2021). Diverging land-use projections cause large variability in their impacts on ecosystems and related indicators for ecosystem services. *Earth System Dynamics*, *12*(1), 327–351. https://doi.org/10.5194/esd-12-327-2021

Bayer, A. D., Lindeskog, M., Pugh, T. A. M., Anthoni, P. M., Fuchs, R., & Arneth, A. (2017). Uncertainties in the land-use flux resulting from land-use change reconstructions and gross land transitions. *Earth System Dynamics*, *8*(1), 91–111. https://doi.org/10.5194/esd-8-91-2017

Bellouin, N., Rae, J., Jones, A., Johnson, C., Haywood, J., & Boucher, O. (2011). Aerosol forcing in the Climate Model Intercomparison Project (CMIP5) simulations by HadGEM2-ES and the role of ammonium nitrate. *Journal of Geophysical Research*, *116*(D20), D20206. https://doi.org/10.1029/2011JD016074

Brienen, R. J. W., Phillips, O. L., Feldpausch, T. R., Gloor, E., Baker, T. R., Lloyd, J., et al. (2015). Long-term decline of the Amazon carbon sink. *Nature*, *519*(7543), 344–348. https://doi.org/10.1038/nature14283

Chen, C., Riley, W. J., Prentice, I. C., & Keenan, T. F. (2022). CO_2 fertilization of terrestrial photosynthesis inferred from site to global scales. *Proceedings of the National Academy of Science U.S.A.*, *119*(10), e2115627119. https://doi.org/10.1073/pnas.2115627119

19449224, 2024, 7, Downloaded from https://agupubs.onlinelibrary.wiley.com/doi/10.1029/2024GB008102 by University Of Illinois At, Wiley Online Library on [22/07/2024]. See the Terms and Conditions (https://onlinelibrary.wiley.com/terms-and-conditions) on Wiley Online Library for rules of use; OA articles are governed by the applicable Creative Commons License

Chini, L., Hurtt, G., Sahajpal, R., Frolking, S., Klein Goldewijk, K., Sitch, S., et al. (2021). Land-use harmonization datasets for annual global carbon budgets. *Earth System Science Data*, *13*(8), 4175–4189. https://doi.org/10.5194/essd-13-4175-2021

Chuvieco, E., Roteta, E., Sali, M., Stroppiana, D., Boettcher, M., Kirches, G., et al. (2022). Building a small fire database for Sub-Saharan Africa from Sentinel-2 high-resolution images. *Science of the Total Environment*, *845*, 157139. https://doi.org/10.1016/j.scitotenv.2022.157139

Collier, N., Hoffman, F. M., Lawrence, D. M., Keppel-Aleks, G., Koven, C. D., Riley, W. J., et al. (2018). The International Land Model Benchmarking (ILAMB) system: Design, theory, and implementation. *Journal of Advances in Modeling Earth Systems*, *10*(11), 2731–2754. https://doi.org/10.1029/2018MS001354

Cramer, W., Kicklighter, D. W., Bondeau, A., Moore, III, B., Churkina, G., Nemry, B., et al. (2001). Comparing global models of terrestrial net primary productivity (NPP): Overview and key results. *Global Change Biology*, *5*(S1), 1–15. https://doi.org/10.1046/j.1365-2486.1999.00009.x

Dai, A., & Trenberth, K. E. (2002). Estimates of freshwater discharge from continents: Latitudinal and seasonal variations. *Journal of Hydrometeorology*, *3*(6), 660–687. https://doi.org/10.1175/1525-7541(2002)003<0660:EOFDFC>2.0.CO;2

Eller, C. B., Rowland, L., Mencuccini, M., Rosas, T., Williams, K., Harper, A., et al. (2020). Stomatal optimization based on xylem hydraulics (SOX) improves land surface model simulation of vegetation responses to climate. *New Phytologist*, *226*(6), 1622–1637. https://doi.org/10.1111/nph.16419

ESA. (2016). *Three global LC maps for the 2000, 2005 and 2010 epochs*. European Space Agency. Retrieved from http://maps.elie.ucl.ac.be/CCI/viewer/index.php

FAO. (2020a). *FAOSTAT Database*. Food and Agriculture Organization of the United Nations. Retrieved from https://www.fao.org/faostat/en/#data/RL

FAO. (2020b). *FAOSTAT Database*. Food and Agriculture Organization of the United Nations. Retrieved from http://www.fao.org/faostat/en/#data/FO

Fisher, J. B., Huntzinger, D. N., Schwalm, C. R., & Sitch, S. (2014). Modeling the terrestrial biosphere. *Annual Review of Environment and Resources*, *39*(1), 15.1–15.33. https://doi.org/10.1146/annurev-environ-012913-093456

Friedlingstein, P., Cox, P., Betts, R., Bopp, L., von Bloh, W., Brovkin, V., et al. (2006). Climate–carbon cycle feedback analysis: Results from the C4MIP model intercomparison. *Journal of Climate*, *19*(14), 3337–3353. https://doi.org/10.1175/jcli3800.1

Friedlingstein, P., Jones, M. W., O'Sullivan, M., Andrew, R. M., Bakker, D. C. E., Hauck, J., et al. (2022a). Global carbon budget 2022. *Earth System Science Data*, *14*, 4811–4900. https://doi.org/10.5194/essd-14-4811-2022

Friedlingstein, P., Jones, M. W., O'Sullivan, M., Andrew, R. M., Bakker, D. C. E., Hauck, J., et al. (2022b). Global carbon budget 2021. *Earth System Science Data*, *14*(4), 1917–2005. https://doi.org/10.5194/essd-14-1917-2022

Ganzenmüller, R., Bultan, S., Winkler, K., Fuchs, R., Zabel, F., & Pongratz, J. (2022). Land-use change emissions based on high-resolution activity data substantially lower than previously estimated. *Environmental Research Letters*, *17*(6), 064050. https://doi.org/10.1088/1748-9326/ac70d8

Gasser, T., & Ciais, P. (2013). A theoretical framework for the net land-to-atmosphere CO_2 flux and its implications in the definition of "emissions from land-use change". *Earth System Dynamics*, *4*(1), 171–186. https://doi.org/10.5194/esd-4-171-2013

Gitz, V., & Ciais, P. (2003). Amplifying effects of land-use change on future atmospheric CO_2 levels. *Global Biogeochemical Cycles*, *17*(1), 1024. https://doi.org/10.1029/2002GB001963

Goll, D. S., Vuichard, N., Maignan, F., Jornet-Puig, A., Sardans, J., Violette, A., et al. (2017). A representation of the phosphorus cycle for ORCHIDEE (revision 4520). *Geoscientific Model Development*, *10*(10), 3745–3770. https://doi.org/10.5194/gmd-10-3745-2017

Grassi, G., House, J., Kurz, W. A., Cescatti, A., Houghton, R. A., Peters, G. P., et al. (2018). Reconciling global model estimates and country reporting of anthropogenic forest CO_2 sinks. *Nature Climate Change*, *8*(10), 914–920. https://doi.org/10.1038/s41558-018-0283-x

Hansen, M. C., Potapov, P. V., Moore, R., Hancher, M., Turubanova, S. A., Tyukavina, A., et al. (2013). High-resolution global maps of 21st-century forest cover change. *Science*, *342*(6160), 850–853. https://doi.org/10.1126/science

Hantson, S., Arneth, A., Harrison, S. P., Kelley, D. I., Prentice, I. C., Rabin, S. S., et al. (2016). The status and challenge of global fire modelling. *Biogeosciences*, *13*(11), 3359–3375. https://doi.org/10.5194/bg-13-3359-2016

Hantson, S., Kelley, D. I., Arneth, A., Harrison, S. P., Archibald, S., Bachelet, D., et al. (2020). Quantitative assessment of fire and vegetation properties in simulations with fire-enabled vegetation models from the Fire Model Intercomparison Project. *Geoscientific Model Development*, *13*(7), 3299–3318. https://doi.org/10.5194/gmd-13-3299-2020

Hardouin, L., Delire, C., Decharme, B., Lawrence, D. M., Nabel, J. E. M. S., Brovkin, V., et al. (2022). Uncertainty in land carbon budget simulated by terrestrial biosphere models: The role of atmospheric forcing. *Environmental Research Letters*, *17*(9), 094033. https://doi.org/10.1088/1748-9326/ac888d

Harper, K. L., Lamarche, C., Hartley, A., Peylin, P., Ottlé, C., Bastrikov, V., et al. (2023). A 29-year time series of annual 300 m resolution plant-functional-type maps for climate models. *Earth System Science Data*, *15*(3), 1465–1499. https://doi.org/10.5194/essd-15-1465-2023

Harris, I., Osborn, T. J., Jones, P., & Lister, D. (2020). Version 4 of the CRU TS monthly high-resolution gridded multivariate climate dataset. *Scientific Data*, *7*(1), 109. https://doi.org/10.1038/s41597-020-0453-3

Hartung, K., Bastos, A., Chini, L., Ganzenmüller, R., Havermann, F., Hurtt, G. C., et al. (2021). Bookkeeping estimates of the net land-use change flux – A sensitivity study with the CMIP6 land-use dataset. *Earth System Dynamics*, *12*(2), 763–782. https://doi.org/10.5194/esd-12-763-2021

Haverd, V., Smith, B., Canadell, J. G., Cuntz, M., Mikaloff-Fletcher, S., Farquhar, G., et al. (2020). Higher than expected CO_2 fertilization inferred from leaf to global observations. *Global Change Biology*, *26*(4), 2390–2402. https://doi.org/10.1111/gcb.14950

Hegglin, M., Kinnison, D., & Lamarque, J.-F. (2016). CCMI nitrogen surface fluxes in support of CMIP6 - Version 2.0. *Earth System Grid Federation*. https://doi.org/10.22033/ESGF/input4MIPs.1125

Heimann, M., Esser, G., Haxeltine, A., Kaduk, J., Kicklighter, D. W., Knorr, W., et al. (1998). Evaluation of terrestrial carbon cycle models through simulations of the seasonal cycle of atmospheric CO_2: First results of a model intercomparison study. *Global Biogeochemical Cycles*, *12*(1), 1–24. https://doi.org/10.1029/97GB01936

Heinrich, V. H. A., Dalagnol, R., Cassol, H. L. G., Rosan, T. M., de Almeida, C. T., Silva Junior, C. H. L., et al. (2021). Large carbon sink potential of secondary forests in the Brazilian Amazon to mitigate climate change. *Nature Communications*, *12*(1), 1785. https://doi.org/10.1038/s41467-021-22050-1

Heinrich, V. H. A., Vancutsem, C., Dalagnol, R., Rosan, T. M., Fawcett, D., Silva-Junior, C. H. L., et al. (2023). The carbon sink of secondary and degraded humid tropical forests. *Nature*, *615*(7952), 436–442. https://doi.org/10.1038/s41586-022-05679-w

Henderson-Sellers, A., Yang, Z.-L., & Dickinson, R. E. (1993). The Project for Intercomparison of Land-surface Parameterization Schemes. *Bulletin of the American Meteorological Society*, *74*(7), 1335–1350. https://doi.org/10.1175/1520-0477(1993)074<1335:TPFIOL>2.0.CO;2

Hersbach, H., Bell, B., Berrisford, P., Hirahara, S., Horányi, A., Muñoz-Sabater, J., et al. (2020). The ERA5 global reanalysis. *The Quarterly Journal of the Royal Meteorological Society*, *146*(730), 1999–2049. https://doi.org/10.1002/qj.3803

19449224, 2024, 7, Downloaded from https://agupubs.onlinelibrary.wiley.com/doi/10.1029/2024GB008102 by University Of Illinois At, Wiley Online Library on [22/07/2024]. See the Terms and Conditions (https://onlinelibrary.wiley.com/terms-and-conditions) on Wiley Online Library for rules of use; OA articles are governed by the applicable Creative Commons License

Houghton, R. A., Hobbie, J. E., Melillo, J. M., Moore, B., Peterson, B. J., Shaver, G. R., & Woodwell, G. M. (1983). Changes in the carbon content of terrestrial biota and soils between 1860 and 1980: A net release of CO_2 to the atmosphere. *Ecological Monographs*, *53*(3), 235–262. https://doi.org/10.2307/1942531

Hubau, W., Lewis, S. L., Phillips, O. L., Affum-Baffoe, K., Beeckman, H., Cuní-Sanchez, A., et al. (2020). Asynchronous carbon sink saturation in African and Amazonian tropical forests. *Nature*, *579*(7797), 80–87. https://doi.org/10.1038/s41586-020-2035-0

Huntingford, C., & Oliver, R. J. (2021). Constraints on the CO_2 fertilization effect emerge. *Nature*, *600*(7888), 224–225. https://doi.org/10.1038/d41586-021-03560-w

Hurtt, G., Chini, L., Sahajpal, R., Frolking, S., Bodirsky, B. L., Calvin, K., et al. (2019a). *Harmonization of global land use change and management for the period 2015–2300, version 20201015*. Earth System Grid Federation. https://doi.org/10.22033/ESGF/input4MIPs.10468

Hurtt, G., Chini, L., Sahajpal, R., Frolking, S., Bodirsky, B. L., Calvin, K., et al. (2019b). *Harmonization of global land use change and management for the period 850–2015, version 20201015*. Earth System Grid Federation. https://doi.org/10.22033/ESGF/input4MIPs.10454

Hurtt, G. C., Chini, L., Sahajpal, R., Frolking, S., Bodirsky, B. L., Calvin, K., et al. (2020). Harmonization of global land use change and management for the period 850–2100 (LUH2) for CMIP6. *Geoscientific Model Development*, *13*(11), 5425–5464. https://doi.org/10.5194/gmd-13-5425-2020

Inness, A., Ades, M., Agustí-Panareda, A., Barré, J., Benedictow, A., Blechschmidt, A.-M., et al. (2019). The CAMS reanalysis of atmospheric composition. *Atmospheric Chemistry and Physics*, *19*(6), 3515–3556. https://doi.org/10.5194/acp-19-3515-2019

INPE. (2020). *Portal TerraBrasilis*. Instituto Nacional de Pesquisas Espaciais (INPE). Retrieved from http://terrabrasilis.dpi.inpe.br

IPCC. (2007). Summary for policymakers. In S. Solomon, D. Qin, M. Manning, Z. Chen, M. Marquis, K. B. Averyt, et al. (Eds.), *Climate Change 2007: The Physical Science Basis. Contribution of Working Group I to the Fourth Assessment Report of the Intergovernmental Panel on Climate Change*. Cambridge University Press.

Jones, M. W., Abatzoglou, J. T., Veraverbeke, S., Andela, N., Lasslop, G., Forkel, M., et al. (2022). Global and regional trends and drivers of fire under climate change. *Reviews of Geophysics*, *60*(3), e2020RG000726. https://doi.org/10.1029/2020rg000726

Joos, F., & Spahni, R. (2008). Rates of change in natural and anthropogenic radiative forcing over the past 20,000 years. *Proceedings of the National Academy of Sciences*, *105*(5), 1425–1430. https://doi.org/10.1073/pnas.0707386105

Jung, M., Reichstein, M., Schwalm, C. R., Huntingford, C., Sitch, S., Ahlström, A., et al. (2017). Compensatory water effects link yearly global land CO_2 sink changes to temperature. *Nature*, *541*(7638), 516–520. https://doi.org/10.1038/nature20780

Kaplan, J. O., & Lau, L. H.-K. (2021). The WGLC global gridded lightning climatology and time series. *Earth System Science Data*, *13*(7), 3219–3237. https://doi.org/10.5194/essd-13-3219-2021

Keeling, C. D., Whorf, T. P., Wahlen, M., & Van der Plichtt, J. (1995). Interannual extremes in the rate of rise of atmospheric carbon dioxide since 1980. *Nature*, *375*(6533), 666–670. https://doi.org/10.1038/375666a0

Keeling, R. F., & Manning, A. C. (2014). 5.15 – Studies of recent changes in atmospheric O_2 content. In H. D. Holland & K. K. Turekian (Eds.), *Treatise on Geochemistry* (2nd ed., pp. 385–404). Elsevier. https://doi.org/10.1016/B978-0-08-095975-7.00420-4

Klein Goldewijk, K., Beusen, A., Doelman, J., & Stehfest, E. (2017). Anthropogenic land use estimates for the Holocene – HYDE 3.2. *Earth System Science Data*, *9*(2), 927–953. https://doi.org/10.5194/essd-9-927-2017

Klein Goldewijk, K., Dekker, S. C., & van Zanden, J. L. (2017). Per-capita estimations of long-term historical land use and the consequences for global change research. *Journal of Land Use Science*, *12*(5), 313–337. https://doi.org/10.1080/1747423X.2017.1354938

Kobayashi, S., Ota, Y., Harada, Y., Ebita, A., Moriya, M., Onoda, H., et al. (2015). The JRA-55 reanalysis: General specifications and basic characteristics. *Journal of the Meteorological Society of Japan*, *93*(1), 5–48. https://doi.org/10.2151/jmsj.2015-001

Le Quéré, C., Raupach, M. R., Canadell, J. G., Marland, G., Bopp, L., Ciais, P., et al. (2009). Trends in the sources and sinks of carbon dioxide. *Nature Geosciences*, *2*(12), 831–836. https://doi.org/10.1038/ngeo689

Li, F., Val Martin, M., Andreae, M. O., Arneth, A., Hantson, S., Kaiser, J. W., et al. (2019). Historical (1700–2012) global multi-model estimates of the fire emissions from the Fire Modeling Intercomparison Project (FireMIP). *Atmospheric Chemistry and Physics*, *19*, 12545–12567. https://doi.org/10.5194/acp-19-12545-2019

Ma, L., Hurtt, G. C., Chini, L. P., Sahajpal, R., Pongratz, J., Frolking, S., et al. (2020). Global rules for translating land-use change (LUH2) to land-cover change for CMIP6 using GLM2. *Geoscientific Model Development*, *13*(7), 3203–3220. https://doi.org/10.5194/gmd-13-3203-2020

McGuire, A. D., Sitch, S., Clein, J. S., Dargaville, R., Esser, G., Foley, J., et al. (2001). Carbon balance of the terrestrial biosphere in the twentieth century: Analyses of CO_2, climate and land use effects with four process-based ecosystem models. *Global Biogeochemical Cycles*, *15*(1), 183–206. https://doi.org/10.1029/2000GB001298

Medlyn, B. E., Zaehle, S., De Kauwe, M. G., Walker, A. P., Dietze, M. C., Hanson, P. J., et al. (2015). Using ecosystem experiments to improve vegetation models. *Nature Climate Change*, *5*(6), 528–534. https://doi.org/10.1038/nclimate2621

Melillo, J. M., Borchers, J., Chaney, J., Fisher, H., Fox, S., Haxeltine, A., et al. (1995). Vegetation/ecosystem modeling and analysis project: Comparing biogeography and biogeochemistry models in a continental-scale study of terrestrial ecosystem responses to climate change and CO_2 doubling. *Global Biogeochemical Cycles*, *9*(4), 407–437. https://doi.org/10.1029/95GB02746

Mercado, L. M., Bellouin, N., Sitch, S., Boucher, O., Huntingford, C., Cox, P. M., et al. (2009). Impact of changes in diffuse radiation on the global land carbon sink. *Nature*, *458*(7241), 1014–1017. https://doi.org/10.1038/nature07949

Nabuurs, G. J., Lindner, M., Verkerk, P. J., Gunia, K., Deda, P., Michalak, R., & Grassi, G. (2013). First signs of carbon sink saturation in European forest biomass. *Nature Climate Change*, *3*(9), 792–796. https://doi.org/10.1038/nclimate1853

Nabuurs, G. J., Schelhaas, M. J., Mohren, G. M. J., & Field, C. B. (2003). Temporal evolution of the European Forest sector carbon sink 1950–1999. *Global Change Biology*, *9*(2), 152–160. https://doi.org/10.1046/j.1365-2486.2003.00570.x

Obermeier, W. A., Nabel, J. E. M. S., Loughran, T., Hartung, K., Bastos, A., Havermann, F., et al. (2021). Modelled land use and land cover change emissions – A spatio-temporal comparison of different approaches. *Earth System Dynamics*, *12*(2), 635–670. https://doi.org/10.5194/esd-12-635-2021

O'Sullivan, M., Friedlingstein, P., Sitch, S., Anthoni, P., Arneth, A., Arora, V. K., et al. (2022). Process-oriented analysis of dominant sources of uncertainty in the land carbon sink. *Nature Communications*, *13*(1), 4781. https://doi.org/10.1038/s41467-022-32416-8

O'Sullivan, M., Zhang, Y., Bellouin, N., Harris, I., Mercado, L. M., Sitch, S., et al. (2021). Aerosol-light interactions reduce the carbon budget imbalance. *Environmental Research Letters*, *16*(12), 124072. https://doi.org/10.1088/1748-9326/ac3b77

Peylin, P., Bousquet, P., Le Quéré, C., Sitch, S., Friedlingstein, P., McKinley, G., et al. (2005). Multiple constraints on regional CO_2 flux variations over land and oceans. *Global Biogeochemical Cycles*, *19*(1), GB1011. https://doi.org/10.1029/2003GB002214

Piao, S., Friedlingstein, P., Ciais, P., Viovy, N., & Demarty, J. (2007). Growing season extension and its impact on terrestrial carbon cycle in the Northern Hemisphere over the past 2 decades. *Global Biogeochemical Cycles*, *21*(3), GB3018. https://doi.org/10.1029/2006GB002888

Piao, S., Wang, X., Wang, K., Li, X., Bastos, A., Canadell, J. G., et al. (2019). Interannual variation of terrestrial carbon cycle: Issues and perspectives. *Global Change Biology*, *26*(1), 300–318. https://doi.org/10.1111/gcb.14884

19449224, 2024, 7, Downloaded from https://agupubs.onlinelibrary.wiley.com/doi/10.1029/2024GB008102 by University Of Illinois At, Wiley Online Library on [22/07/2024]. See the Terms and Conditions (https://onlinelibrary.wiley.com/terms-and-conditions) on Wiley Online Library for rules of use; OA articles are governed by the applicable Creative Commons License

Plummer, S., Lecomte, P., & Doherty, M. (2017). The ESA Climate Change Initiative (CCI): A European contribution to the generation of the Global Climate Observing System. *Remote Sensing of Environment*, *203*, 2–8. https://doi.org/10.1016/j.rse.2017.07.014

Pongratz, J., Dolman, H., Don, A., Erb, K.-H., Fuchs, R., Herold, M., et al. (2017). Models meet data: Challenges and opportunities in implementing land management in Earth System Models. *Global Change Biology*, *24*(4), 1470–1487. https://doi.org/10.1111/gcb.13988

Pongratz, J., Reick, C. H., Houghton, R., & House, J. (2014). Terminology as a key uncertainty in net land use and land cover change carbon flux estimates. *Earth System Dynamics*, *5*(1), 177–195. https://doi.org/10.5194/esd-5-177-2014

Pongratz, J., Schwingshackl, C., Bultan, S., Obermeier, W., Havermann, F., & Guo, S. (2021). Land use effects on climate: Current state, recent progress, and emerging topics. *Current Climate Change Reports*, *7*(4), 99–120. https://doi.org/10.1007/s40641-021-00178-y

Poulter, B., Frank, D., Ciais, P., Myneni, R., Andela, N., Bi, J., et al. (2014). Contribution of semi-arid ecosystems to interannual variability of the global carbon cycle. *Nature*, *509*(7502), 600–603. https://doi.org/10.1038/nature13376

Prentice, I. C., Bondeau, A., Cramer, W., Harrison, S. P., Hickler, T., Lucht, W., et al. (2007). Dynamic global vegetation modeling: Quantifying terrestrial ecosystem responses to large-scale environmental change. In J. G. Canadell, D. E. Pataki, & L. F. Pitelka (Eds.), *Terrestrial Ecosystems in a Changing World. Global Change — The IGBP Series*. Springer. https://doi.org/10.1007/978-3-540-32730-1_15

Rabin, S. S., Melton, J. R., Lasslop, G., Bachelet, D., Forrest, M., Hantson, S., et al. (2017). The Fire Modeling Intercomparison Project (FireMIP), phase 1: Experimental and analytical protocols with detailed model descriptions. *Geoscientific Model Development*, *10*(3), 1175–1197. https://doi.org/10.5194/gmd-10-1175-2017

Ramo, R., Roteta, E., Bistinas, I., van Wees, D., Bastarrika, A., Chuvieco, E., & van der Werf, G. R. (2021). African burned area and fire carbon emissions are strongly impacted by small fires undetected by coarse resolution satellite data. *Proceedings of the National Academy of Sciences*, *118*(9), e2011160118. https://doi.org/10.1073/pnas.2011160118

Roderick, M. L., Farquhar, G. D., Berry, S. L., & Noble, I. R. (2001). On the direct effect of clouds and atmospheric particles on the productivity and structure of vegetation. *Oecologia*, *129*(1), 21–30. https://doi.org/10.1007/s004420100760

Rosan, T. M., Goldewijk, K. K., Ganzenmüller, R., O'Sullivan, M., Pongratz, J., Mercado, L. M., et al. (2021). A multi-data assessment of land use and land cover emissions from Brazil during 2000–2019. *Environmental Research Letters*, *16*(7), 074004. https://doi.org/10.1088/1748-9326/ac08c3

Ruehr, S., Keenan, T. F., Williams, C., Zhou, Y., Lu, X., Bastos, A., et al. (2023). Evidence and attribution of the enhanced land carbon sink. *Nature Reviews Earth & Environment*, *4*(8), 518–534. https://doi.org/10.1038/s43017-023-00456-3

Saatchi, S. S., Harris, N. L., Brown, S., Lefsky, M., Mitchard, E. T. A., Salas, W., et al. (2011). Benchmark map of forest carbon stocks in tropical regions across three continents. *Proceedings of the National Academy of Sciences*, *108*(24), 9899–9904. https://doi.org/10.1073/pnas.1019576108

Santoro, M., & Cartus, O. (2021). *ESA Biomass Climate Change Initiative (Biomass_CCI): Global datasets of forest above-ground biomass for the years 2010, 2017 and 2018, v3*. NERC EDS Centre for Environmental Data Analysis. https://doi.org/10.5285/5f331c418e9f4935b8eb1b836f8a91b8

Sato, M., Hansen, J. E., McCormick, M. P., & Pollack, J. B. (1993). Stratospheric aerosol optical depths, 1850–1990. *Journal of Geophysical Research*, *98*(D12), 22987–22994. https://doi.org/10.1029/93JD02553

Saunois, M., Stavert, A. R., Poulter, B., Bousquet, P., Canadell, J. G., Jackson, R. B., et al. (2020). The global methane budget 2000–2017. *Earth System Science Data*, *12*(3), 1561–1623. https://doi.org/10.5194/essd-12-1561-2020

Seiler, C., Melton, J. R., Arora, V. K., Sitch, S., Friedlingstein, P., Anthoni, P., et al. (2022). Are terrestrial biosphere models fit for simulating the global land carbon sink? *Journal of Advances in Modeling Earth Systems*, *14*(5), e2021MS002946. https://doi.org/10.1029/2021MS002946

Silva Junior, C. H., Aragão, L. E., Anderson, L. O., Fonseca, M. G., Shimabukuro, Y. E., Vancutsem, C., et al. (2020). Persistent collapse of biomass in Amazonian forest edges following deforestation leads to unaccounted carbon losses. *Science Advances*, *6*(40), eaaz8360. https://doi.org/10.1126/sciadv.aaz8360

Sitch, S., Brovkin, V., von Bloh, W., Van Vuuren, D., Eickhout, B., & Ganopolski, A. (2005). Impacts of future land cover on atmospheric CO_2 and climate. *Global Biogeochemical Cycles*, *19*(2), GB2013. https://doi.org/10.1029/2004GB002311

Sitch, S., Friedlingstein, P., Gruber, N., Jones, S., Murray-Tortarolo, G., Ahlström, A., et al. (2015). Recent trends and drivers of regional sources and sinks of carbon dioxide. *Biogeosciences*, *12*(3), 653–679. https://doi.org/10.5194/bg-12-653-2015

Souza, C. M., Jr., Shimbo, J. Z., Rosa, M. R., Parente, L. L., Alencar, A. A., Rudorff, B. F., et al. (2020). Reconstructing three decades of land use and land cover changes in Brazilian biomes with Landsat archive and earth engine. *Remote Sensing*, *12*(17), 2735. https://doi.org/10.3390/rs12172735

Thomason, L. W., Ernest, N., Millán, L., Rieger, L., Bourassa, A., Vernier, J.-P., et al. (2018). A global space-based stratospheric aerosol climatology: 1979–2016. *Earth System Science Data*, *10*(1), 469–492. https://doi.org/10.5194/essd-10-469-2018

Thornton, P. E., Lamarque, J. F., Rosenbloom, N. A., & Mahowald, N. M. (2007). Inclusion of carbon-nitrogen cycle coupling on land model response to CO_2 fertilization and climate variability. *Global Biogeochemical Cycles*, *21*(4), GB4018. https://doi.org/10.1029/2006GB002868

Thurner, M., Beer, C., Santoro, M., Carvalhais, N., Wutzler, T., Schepaschenko, D., et al. (2014). Carbon stock and density of boreal and temperate forests. *Global Ecology and Biogeography*, *23*(3), 297–310. https://doi.org/10.1111/geb.12125

Tian, H., Bian, Z., Shi, H., Qin, X., Pan, N., Lu, C., et al. (2022). History of anthropogenic Nitrogen inputs (HaNi) to the terrestrial biosphere: A 5 arcmin resolution annual dataset from 1860 to 2019. *Earth System Science Data*, *14*(10), 4551–4568. https://doi.org/10.5194/essd-14-4551-2022

Tian, H., Melillo, J., Kicklighter, D. W., McGuire, A. D., Helfrich III, J. V. K., Moore III, B., & Vörösmarty, C. J. (1998). Effect of interannual climate variability on carbon storage in Amazonian ecosystems. *Nature*, *396*(6712), 664–667. https://doi.org/10.1038/25328

Tian, H., Xu, R., Canadell, J. G., Thompson, R. L., Winiwarter, W., Suntharalingam, P., et al. (2020). A comprehensive quantification of global nitrous oxide sources and sinks. *Nature*, *586*(7828), 248–256. https://doi.org/10.1038/s41586-020-2780-0

Tian, H., Yang, J., Lu, C., Xu, R., Canadell, J. G., Jackson, R. B., et al. (2018). The Global N_2O model intercomparison project. *Bulletin of the American Meteorological Society*, *99*(6), 1231–1251. https://doi.org/10.1175/BAMS-D-17-0212.1

Tian, H., Yang, J., Xu, R., Lu, C., Canadell, J. G., Davidson, E. A., et al. (2019). Global soil nitrous oxide emissions since the preindustrial era estimated by an ensemble of terrestrial biosphere models: Magnitude, attribution, and uncertainty. *Global Change Biology*, *25*(2), 640–659. https://doi.org/10.1111/gcb.14514

Townsend, A. R., Braswell, B. H., Holland, E. A., & Penner, J. E. (1996). Spatial and temporal patterns of carbon storage due to deposition of fossil fuel nitrogen. *Ecological Applications*, *6*(3), 806–814. https://doi.org/10.2307/2269486

Tramontana, G., Jung, M., Schwalm, C. R., Ichii, K., Camps-Valls, G., Raduly, B., et al. (2016). Predicting carbon dioxide and energy fluxes across global FLUXNET sites with regression algorithms. *Biogeosciences*, *13*(14), 4291–4313. https://doi.org/10.5194/bg-13-4291-2016

Walker, A., De Kauwe, M. G., Bastos, A., Belmecheri, S., Georgiou, K., Keeling, R. F., et al. (2020). Integrating the evidence for a terrestrial carbon sink caused by increasing atmospheric CO_2. *New Phytologist*, *229*(5), 2413–2445. https://doi.org/10.1111/nph.16866

19449224, 2024, 7, Downloaded from https://agupubs.onlinelibrary.wiley.com/doi/10.1029/2024GB008102 by University Of Illinois At, Wiley Online Library on [22/07/2024]. See the Terms and Conditions (https://onlinelibrary.wiley.com/terms-and-conditions) on Wiley Online Library for rules of use; OA articles are governed by the applicable Creative Commons License

Wang, S., Zhang, Y., Ju, W., Chen, J. M., Ciais, P., Cescatti, A., et al. (2020). Recent global decline of CO_2 fertilization effects on vegetation photosynthesis. *Science*, *370*(6522), 1295–1300. https://doi.org/10.1126/science.abb7772
Wang, X., Gao, Y., Jeong, S., Ito, A., Bastos, A., Poulter, B., et al. (2024). The greenhouse gas budget of terrestrial ecosystems in East Asia since 2000. *Global Biogeochemical Cycles*, *38*(2), e2023GB007865. https://doi.org/10.1029/2023GB007865
Wang, Y., Sperry, J. S., Anderegg, W. R. L., Venturas, M. D., & Trugman, A. T. (2020). A theoretical and empirical assessment of stomatal optimization modeling. *New Phytologist*, *227*(2), 311–325. https://doi.org/10.1111/nph.16572
Wang, Y. P., Houlton, B. Z., & Field, C. B. (2007). A model of biogeochemical cycles of carbon, nitrogen, and phosphorus including symbiotic nitrogen fixation and phosphatase production. *Global Biogeochemical Cycles*, *21*, 1–15. https://doi.org/10.1029/2006GB002797
Wang, Y. P., Law, R. M., & Pak, B. (2010). A global model of carbon, nitrogen and phosphorus cycles for the terrestrial biosphere. *Biogeosciences*, *7*, 2261–2282. https://doi.org/10.5194/bg-7-2261-2010
Wieder, W. R., Boehnert, J., & Bonan, G. B. (2014). Evaluating soil biogeochemistry parameterizations in Earth system models with observations. *Global Biogeochemical Cycles*, *28*(3), 211–222. https://doi.org/10.1002/2013GB004665
Wieder, W. R., Boehnert, J., Bonan, G. B., & Langseth, M. (2014). Regridded Harmonized World Soil Database v1.2 [Dataset]. *Oak Ridge National Laboratory Distributed Active Archive Center*. https://doi.org/10.3334/ORNLDAAC/1247
Winkler, K., Yang, H., Ganzenmüller, R., Fuchs, R., Ceccherini, G., Duveiller, G., et al. (2023). Changes in land use and management led to a decline in Eastern Europe's terrestrial carbon sink. *Communications Earth & Environment*, *4*(1), 237. https://doi.org/10.1038/s43247-023-00893-4
WMO. (2023). Global Greenhouse Gas Watch (GGGW). Retrieved from https://public.wmo.int/en/our-mandate/focus-areas/environment/greenhouse-gases/global-greenhouse-gas-monitoring-infrastructure
Wu, Z., Ahlström, A., Smith, B., Ardö, J., Eklundh, L., Fensholt, R., et al. (2017). Climate data induced uncertainty in model-based estimations of terrestrial primary productivity. *Environmental Research Letters*, *12*(6), 064013. https://doi.org/10.1088/1748-9326/aa6fd8
Yang, H., Ciais, P., Frappart, F., Li, X., Brandt, M., Fensholt, R., et al. (2023). Global increase in biomass carbon stock dominated by growth of northern young forests over past decade. *Nature Geoscience*, *16*(10), 886–892. https://doi.org/10.1038/s41561-023-01274-4
Yang, H., Ciais, P., Santoro, M., Huang, Y., Li, W., Wang, Y., et al. (2020). Comparison of forest above-ground biomass from dynamic global vegetation models with spatially explicit remotely sensed observation-based estimates. *Global Change Biology*, *26*(7), 3997–4012. https://doi.org/10.1111/gcb.15117
Yang, X., Thornton, P. E., Ricciuto, D. M., & Post, W. M. (2014). The role of phosphorus dynamics in tropical forests – A modeling study using CLM-CNP. *Biogeosciences*, *11*(6), 1667–1681. https://doi.org/10.5194/bg-11-1667-2014
Yu, Z., Ciais, P., Piao, S., Houghton, R. A., Lu, C., Tian, H., et al. (2022). Forest expansion dominates China's land carbon sink since 1980. *Nature Communications*, *13*(1), 5374. https://doi.org/10.1038/s41467-022-32961-2
Zaehle, S., & Friend, A. D. (2010). Carbon and nitrogen cycle dynamics in the O-CN land surface model: 1. Model description, site-scale evaluation, and sensitivity to parameter estimates. *Global Biogeochemical Cycles*, *24*(1), GB1005. https://doi.org/10.1029/2009gb003521
Zaehle, S., Friend, A. D., & Friedlingstein, P. (2010). Terrestrial nitrogen feedbacks may accelerate future climate change. *Geophysical Research Letters*, *37*(1), L01401. https://doi.org/10.1029/2009GL041345
Zheng, B., Ciais, P., Chevallier, F., Chuvieco, E., Chen, Y., & Yang, H. (2021). Increasing forest fire emissions despite the decline in global burned area. *Science Advances*, *7*(39), eabh2646. https://doi.org/10.1126/sciadv.abh2646
Zon, R., & Sparhawk, W. N. (1923). *Forest resources of the world* (Vol. 1, p. 493). McGraw-Hill.

References From the Supporting Information

Arora, V. K., Seiler, C., Wang, L., & Kou-Giesbrecht, S. (2023). Towards an ensemble-based evaluation of land surface models in light of uncertain forcings and observations. *Biogeosciences*, *20*(7), 1313–1355. https://doi.org/10.5194/bg-20-1313-2023
Calle, L., & Poulter, B. (2021). Ecosystem age-class dynamics and distribution in the LPJ-wsl v2.0 global ecosystem model. *Geoscientific Model Development*, *14*(5), 2575–2601. https://doi.org/10.5194/gmd-14-2575-2021
Haverd, V., Smith, B., Nieradzik, L., Briggs, P. R., Woodgate, W., Trudinger, C. M., et al. (2018). A new version of the CABLE land surface model (Subversion revision r4601) incorporating land use and land cover change, woody vegetation demography, and a novel optimisation-based approach to plant coordination of photosynthesis. *Geoscientific Model Development*, *11*(7), 2995–3026. https://doi.org/10.5194/gmd-11-2995-2018
Ito, A. (2019). Disequilibrium of terrestrial ecosystem CO_2 budget caused by disturbance-induced emissions and non-CO_2 carbon export flows: A global model assessment. *Earth System Dynamics*, *10*(4), 685–709. https://doi.org/10.5194/esd-10-685-2019
Jung, M., Henkel, K., Herold, M., & Churkina, G. (2006). Exploiting synergies of global land cover products for carbon cycle modeling. *Remote Sensing of Environment*, *101*(4), 534–553. https://doi.org/10.1016/j.rse.2006.01.020
Kato, E., Kinoshita, T., Ito, A., Kawamiya, M., & Yamagata, Y. (2013). Evaluation of spatially explicit emission scenario of land-use change and biomass burning using a process-based biogeochemical model. *Journal of Land Use Science*, *8*(1), 104–122. https://doi.org/10.1080/1747423x.2011.628705
Lawrence, D. M., Hurtt, G. C., Arneth, A., Brovkin, V., Calvin, K. V., Jones, A. D., et al. (2016). The Land Use Model Intercomparison Project (LUMIP): Rationale and experimental design. *Geoscientific Model Development*, *9*(9), 2973–2998. https://doi.org/10.5194/gmd-5199-2973-2016
Lawrence, D. M., Fisher, R. A., Koven, C. D., Oleson, K. W., Swenson, S. C., Bonan, G., et al. (2019). The community land model version 5: Description of new features, benchmarking, and impact of forcing uncertainty. *Journal of Advances in Modeling Earth Systems*, *11*(12), 4245–4287. https://doi.org/10.1029/2018ms001583
Lienert, S., & Joos, F. (2018). A Bayesian ensemble data assimilation to constrain model parameters and land-use carbon emissions. *Biogeosciences*, *15*(9), 2909–2930. https://doi.org/10.5194/bg-15-2909-2018
Lindeskog, M., Arneth, A., Bondeau, A., Waha, K., Seaquist, J., Olin, S., & Smith, B. (2013). Implications of accounting for land use in simulations of ecosystem carbon cycling in Africa. *Earth System Dynamics*, *4*(2), 385–407. https://doi.org/10.5194/esd-4-385-2013
Lu, C., & Tian, H. (2017). Global nitrogen and phosphorus fertilizer use for agriculture production in the past half century: Shifted hot spots and nutrient imbalance. *Earth System Science Data*, *9*(1), 181–192. https://doi.org/10.5194/essd-9-181-2017
Meiyappan, P., & Jain, A. K. (2012). Three distinct global estimates of historical land-cover change and land-use conversions for over 200 years. *Frontiers of Earth Science*, *6*(2), 122–139. https://doi.org/10.1007/s11707-012-0314-2
Meiyappan, P., Jain, A. K., & House, J. I. (2015). Increased influence of nitrogen limitation on CO_2 emissions from future land use and land use change. *Global Biogeochemical Cycles*, *29*(9), 1524–1548. https://doi.org/10.1002/2015gb005086

19449224, 2024, 7, Downloaded from https://agupubs.onlinelibrary.wiley.com/doi/10.1029/2024GB008102 by University Of Illinois At, Wiley Online Library on [22/07/2024]. See the Terms and Conditions (https://onlinelibrary.wiley.com/terms-and-conditions) on Wiley Online Library for rules of use; OA articles are governed by the applicable Creative Commons License

Melton, J. R., Arora, V. K., Wisernig-Cojoc, E., Seiler, C., Fortier, M., Chan, E., & Teckentrup, L. (2020). Classic v1.0: The open-source community successor to the Canadian Land Surface Scheme (CLASS) and the Canadian Terrestrial Ecosystem Model (CTEM) – Part 1: Model framework and site-level performance. *Geoscientific Model Development*, *13*(6), 2825–2850. https://doi.org/10.5194/gmd-13-2825-2020

Olin, S., Lindeskog, M., Pugh, T. A. M., Schurgers, G., Wärlind, D., Mishurov, M., et al. (2015). Soil carbon management in large-scale Earth system modelling: Implications for crop yields and nitrogen leaching. *Earth System Dynamics*, *6*(2), 745–768. https://doi.org/10.5194/esd-6-745-2015

Pan, S., Tian, H., Dangal, S. R. S., Ouyang, Z., Lu, C., Yang, J., et al. (2015). Impacts of climate variability and extremes on global net primary production in the first decade of the 21st century. *Journal of Geographical Sciences*, *25*(9), 1027–1044. https://doi.org/10.1007/s11442-015-1217-4

Poulter, B., MacBean, N., Hartley, A., Khlystova, I., Arino, O., Betts, R., et al. (2015). Plant functional type classification for earth system models: Results from the European Space Agency's Land Cover Climate Change Initiative. *Geoscientific Model Development*, *8*(7), 2315–2328. https://doi.org/10.5194/gmd-8-2315-2015

Prentice, I. C., Cramer, W., Harrison, S. P., Leemans, R., Monserud, R. A., & Solomon, A. M. (1992). A global biome model based on plant physiology and dominance, soil properties and climate. *Journal of Biogeography*, *19*(2), 117–134. https://doi.org/10.2307/2845499

Reick, C., Gayler, V., Goll, D., Hagemann, S., Heidkamp, M., Nabel, J., et al. (2021). *JSBACH 3 – The land component of the MPI Earth System Model: Documentation of version 3.2* (Technical Report). MPI für Meteorologie.

Rubel, F., Brugger, K., Haslinger, K., & Auer, I. (2017). The climate of the European Alps: Shift of very high resolution Köppen-Geiger climate zones 1800–2100. *Meteorologische Zeitschrift*, *26*(2), 115–125. https://doi.org/10.1127/metz/2016/0816

Sitch, S., Smith, B., Prentice, I. C., Arneth, A., Bondeau, A., Cramer, W., et al. (2003). Evaluation of ecosystem dynamics, plant geography and terrestrial carbon cycling in the LPJ dynamic global vegetation model. *Global Change Biology*, *9*(2), 161–185. https://doi.org/10.1046/j.1365-2486.2003.00569.x

Smith, B., Wårlind, D., Arneth, A., Hickler, T., Leadley, P., Siltberg, J., & Zaehle, S. (2014). Implications of incorporating N cycling and N limitations on primary production in an individual-based dynamic vegetation model. *Biogeosciences*, *11*(7), 2027–2054. https://doi.org/10.5194/bg-11-2027-2014

Still, C. J., Cotton, J. M., Griffith, D. M., Strömberg, C. A. E., & Forrestel, E. J. (2018). Assessing Earth System Model predictions of C_4 grass cover in North America: From the glacial era to the end of this century. *Global Ecology and Biogeography*, *24*(3), 304–313. https://doi.org/10.1111/geb.12265

Stocker, B. D., Feissli, F., Strassmann, K. M., Spahni, R., & Joos, F. (2014). Past and future carbon fluxes from land use change, shifting cultivation and wood harvest. *Tellus B*, *66*(1), 23188. https://doi.org/10.3402/tellusb.v66.23188

Tian, H., Chen, G., Lu, C., Xu, X., Hayes, D. J., Ren, W., et al. (2015). North American terrestrial CO_2 uptake largely offset by CH_4 and N_2O emissions: Toward a full accounting of the greenhouse gas budget. *Climate Change*, *129*(3–4), 413–426. https://doi.org/10.1007/s10584-014-1072-9

Vuichard, N., Messina, P., Luyssaert, S., Guenet, B., Zaehle, S., Ghattas, J., et al. (2019). Accounting for carbon and nitrogen interactions in the global terrestrial ecosystem model ORCHIDEE (trunk version, rev 4999): Multi-scale evaluation of gross primary production. *Geoscientific Model Development*, *12*(11), 4751–4779. https://doi.org/10.5194/gmd-12-4751-2019

Walker, A. P., Quaife, T., Bodegom, P. M., De Kauwe, M. G., Keenan, T. F., Joiner, J., et al. (2017). The impact of alternative trait-scaling hypotheses for the maximum photosynthetic carboxylation rate (V_{cmax}) on global gross primary production. *New Phytologist*, *215*(4), 1370–1386. https://doi.org/10.1111/nph.14623

Wang, D., Ren, P., Xia, X., Fan, L., Qin, Z., Chen, X., & Yuan, W. (2024). National forest carbon harvesting and allocation dataset for the period 2003 to 2018. *Earth System Science Data*. https://doi.org/10.5194/essd-2023-309

Wiltshire, A. J., Burke, E. J., Chadburn, S. E., Jones, C. D., Cox, P. M., Davies-Barnard, T., et al. (2021). JULES-CN: A coupled terrestrial carbon–nitrogen scheme (JULES vn5.1). *Geoscientific Model Development*, *14*(4), 2161–2186. https://doi.org/10.5194/gmd-14-2161-2021

Xu, R., Tian, H., Lu, C., Pan, S., Chen, J., Yang, J., & Zhang, B. (2017). Preindustrial nitrous oxide emissions from the land biosphere estimated by using a global biogeochemistry model. *Climate of the Past*, *13*(7), 977–990. https://doi.org/10.5194/cp-13-977-2017

Yuan, W., Liu, D., Dong, W., Liu, S., Zhou, G., Yu, G., et al. (2014). Multiyear precipitation reduction strongly decreases carbon uptake over northern China. *Journal of Geophysical Research: Biogeosciences*, *119*(5), 881–896. https://doi.org/10.1002/2014jg002608

Zhang, B., Tian, H., Lu, C., Dangal, S. R., Yang, J., & Pan, S. (2017). Global manure nitrogen production and application in cropland during 1860–2014: A 5 arcmin gridded global dataset for Earth system modeling. *Earth System Science Data*, *9*(2), 667–678. https://doi.org/10.5194/essd-9-667-2017

19449224, 2024, 7, Downloaded from https://agupubs.onlinelibrary.wiley.com/doi/10.1029/2024GB008102 by University Of Illinois At, Wiley Online Library on [22/07/2024]. See the Terms and Conditions (https://onlinelibrary.wiley.com/terms-and-conditions) on Wiley Online Library for rules of use; OA articles are governed by the applicable Creative Commons License